Summer 8-31-2005

Synthesis and characterization of polymer nanocomposites

Nirav S. Patel
New Jersey Institute of Technology

ABSTRACT

SYNTHESIS AND CHARACTERIZATION OF POLYMER NANOCOMPOSITES

by
Nirav S. Patel

Polymer nanocomposites were produced by solution mixing of a commercial flexible acrylic polymer paint, with nanofillers of different size, shape, aspect ratio and purity such as hydrotalcite (HT), sodium montmorillonite (MMT), single wall carbon nanotubes (SWNT) and fullerenes (FUL), at 5 and 10 wt% loading. Structural characteristics and mechanical, thermal and barrier properties of the nanocomposites were characterized by different techniques and compared to those of the unfilled polymer.

The presence of partially exfoliated and intercalated nanoplatelets in the polymer resulted in increased 2% secant tensile modulus, and decreased tensile strength and elongation at break, to different extents. While the presence of SWNT improved the mechanical properties of the polymer, the presence of FUL hampered the mechanical properties. Storage modulus of the polymer was also improved in the presence of 10 wt% MMT and SWNT. While moderate changes in the T_g were observed in the presence of fillers the thermal stability of the polymer was not improved by their presence. The presence of all impermeable filler particles in the polymer improves its water vapor barrier property. Significant differences in the properties of different composites when compared to those of the unfilled polymer are attributed to the variations in microstructure and properties, which greatly depend on the aspect ratio, surface area, inherent properties, orientation and extent of interactions of the nanofillers with the acrylic polymer.

SYNTHESIS AND CHARACTERIZATION OF POLYMER NANOCOMPOSITES

by
Nirav S. Patel

A Thesis
Submitted to the Faculty of
New Jersey Institute of Technology
In Partial Fulfillment of the Requirements for the Degree of
Master of Science in Chemical Engineering

Otto H. York Department of Chemical Engineering

August 2005

APPROVAL PAGE

SYNTHESIS AND CHARACTERIZATION OF POLYMER NANOCOMPOSITES

Nirav S. Patel

Dr. Marino Xanthos, Thesis Advisor — Date
Professor of Chemical Engineering, NJIT

Dr. Roman Dubrovsky, Committee Member — Date
Associate Professor of Mechanical Engineering, NJIT

Dr. Zafar Iqbal, Committee Member — Date
Research Professor of Chemistry and Environmental Science, NJIT

BIOGRAPHICAL SKETCH

Author: Nirav S. Patel

Degree: Master of Science

Date: August 2005

Undergraduate and Graduate Education:

- Master of Science in Chemical Engineering,
  New Jersey Institute of Technology, Newark, NJ, 2005

- Bachelor of Engineering in Chemical Engineering,
  Rashtreeya Vidyalaya College of Engineering, Bangalore, Karnataka, India, 2003

Major: Chemical Engineering

This thesis is dedicated to my family
for their unending love and encouragement

ACKNOWLEDGEMENT

I start by expressing my sincere appreciation to my advisor, Dr. Marino Xanthos, for his dedication, patience and wisdom throughout the length of this study and the preparation of this thesis, and without whose guidance this research would not be possible. It was a great privilege to have him as my mentor.

I am grateful to Dr. Roman Dubrovsky and Dr. Zafar Iqbal for agreeing to be a part of my work. I appreciate their input, and I thank them for their constructive and timely support.

I would like to thank Dr. Victor Tan of PPI for his guidance and help with the tensile modulus experiments and Dr. Gopakumar T.G. of PPI for his help with the XRD and other experiments.

I would also like to thank my colleagues and friends, Georgia Chouzouri and Ku-Il Park for all their emotional support and caring. I deeply appreciate their invaluable assistance and cooperation.

Lastly, I take this opportunity to sincerely thank my family and friends for their love and understanding.

TABLE OF CONTENTS

Chapter		Page
1	INTRODUCTION	1
2	POLYMER COMPOSITES WITH NANOFILLERS	3
	2.1 General	3
	2.2 Composites with Nanoplatelets	11
	2.2.1 Montmorillonite Clays	13
	2.2.2 Hydrotalcite	15
	2.3 Composites with Carbon Allotropes	16
	2.3.1 Carbon Nanotubes	16
	2.3.2 Fullerenes	20
3	EXPERIMENTAL	21
	3.1 Materials	21
	3.1.1 Acrylic Paint Polymer	21
	3.1.2 Hydrotalcite	21
	3.1.3 Sodium Montmorillonite	22
	3.1.4 Carbon Nanotubes	23
	3.1.5 Fullerenes	25
	3.2 Processing of Composites	27
	3.3 Testing and Characterization	28
	3.3.1 Scanning Electron Microscopy	28
	3.3.2 Wide Angle X-Ray Diffraction	28

TABLE OF CONTENTS
(Continued)

Chapter		Page
	3.3.3 Mechanical Properties	29
	3.3.4 Thermal Properties	29
	3.3.5 Barrier Properties	30
4	RESULTS AND DISCUSION	31
	4.1 Scanning Electron Microscopy of Fillers and Composites	31
	4.2 Wide Angle X-Ray Diffraction of Fillers and Composites	45
	4.3 Mechanical Properties	49
	4.3.1 Tensile Properties	50
	4.3.2 Dynamic Mechanical Analysis	56
	4.4 Thermal Analysis of Fillers and Composites	58
	4.4.1 Differential Scanning Calorimetric Analysis	58
	4.4.2 Thermogravimetric Analysis	59
	4.5 Barrier Properties	65
5	CONCLUSION	68
APPENDIX A	ENERGY DISPERSIVE X-RAY PLOTS	72
APPENDIX B	DIFFERENTIAL SCANNING CALORIMETRY THERMOGRAMS	75
APPENDIX C	WATER VAPOR TRANSMISSION PLOTS	79
REFERENCES		85

LIST OF TABLES

Table		Page
2.1	Particle Morphology of Fillers.....	4
2.2	Strength Equations for Short Fibers and Flake Composites.....	9
3.1	Properties of Carbon Nanotubes.....	24
4.1	Mechanical Properties of PACR and its Nanocomposites in the Draw Down Direction.....	51
4.2	Mechanical Properties of PACR and its Nanocomposites Perpendicularly to the Draw Down Direction.....	55
4.3	Apparent DSC Glass Transition Temperature of PACR and its Nanocomposites.....	59
4.4	WVTR of PACR and its Nanocomposites with 5 wt% loading.....	65

LIST OF FIGURES

Figure		Page
2.1	Schematic representation of distribution and dispersion of fillers.....	5
2.2	Illustration of Nielsen's tortuous path model for barrier enhancement of composite.....	11
2.3	Schematic illustration of intercalated, semi-exfoliated and exfoliated polymer-clay nanocomposites.....	13
3.1	Molecular structure of hydrotalcite.....	22
3.2	Molecular structure of sodium montmorillonite.....	23
3.3	Schematic picture of multi walled carbon nanotube.....	24
3.4	Schematic picture of single walled carbon nanotube.....	24
3.5	Buckminsterfullerene image.....	25
4.1	SEM images of cryofractured crossection of PHT – 5.....	32
4.2	SEM images of tensile fractured crossection of PHT – 5.....	33
4.3	SEM images of as used HT.....	35
4.4	SEM image of cryofractured crossection of PMMT – 5.....	37
4.5	SEM images of tensile fractured crossection of PMMT – 5.....	37
4.6	SEM images of as used MMT.....	38
4.7	SEM images of cryofractured crossection of PSWNT – 5.....	40
4.8	SEM images of tensile fractured crossection of PSWNT – 5.....	40
4.9	SEM images of as used SWNT.....	42
4.10	SEM images of as used FUL.....	44
4.11	WAXRD patterns of PACR, HT and PHT – 5.....	46

LIST OF FIGURES
(Continued)

Figure		Page
4.12	WAXRD patterns of PACR, MMT and PMMT – 5.....	47
4.13	WAXRD patterns of PACR, SWNT and PSWNT – 5.....	48
4.14	WAXRD patterns of PACR, FUL and PFUL – 5.....	49
4.15	Relative tensile strength at break of PACR and its composites.....	51
4.16	Relative elongation at break of PACR and it composites.....	52
4.17	Relative 2% secant modulus of PACR and its composites.....	52
4.18	Dynamic mechanical spectra of storage modulus for PACR, PMMT – 10 and PSWNT – 10.....	57
4.19	Dynamic mechanical spectra of tanδ for PACR, PMMT – 10 and PSWNT – 10.....	58
4.20	TGA thermograms of PACR, HT and PHT – 5.....	61
4.21	TGA thermograms of PACR, MMT and PMMT – 5.....	61
4.22	TGA thermograms of PACR, PHT – 5 and PMMT – 5.....	62
4.23	TGA thermograms of PACR, SWNT and PSWNT – 5.....	63
4.24	TGA thermograms of PACR, FUL and PFUL – 5.....	64
4.25	TGA thermograms of PACR, PFUL – 5 and PSWNT – 5.....	64
A.1	EDX result of hydrotalcite sample, used as filler.....	73
A.2	EDX result of montmorillonite sample, used as filler.....	73
A.3	EDX result of carbon nanotube sample, used as filler.....	74
A.4	EDX result of fullerene sample, used as filler.....	74
B.1	DSC thermogram of PACR.....	76

LIST OF FIGURES
(Continued)

Figure		Page
B.2	DSC thermogram of PHT – 5	76
B.3	DSC thermogram of PMMT – 5	77
B.4	DSC thermogram of PSWNT – 5	77
B.5	DSC thermogram of PFUL – 5	78
C.1	WVT plot of PACR	80
C.2	WVT plot of PACR	80
C.3	WVT plot of PHT – 5	81
C.4	WVT plot of PHT – 5	81
C.5	WVT plot of PMMT – 5	82
C.6	WVT plot of PMMT – 5	82
C.7	WVT plot of PSWNT – 5	83
C.8	WVT plot of PSWNT – 5	83
C.9	WVT plot of PFUL – 5	84

CHAPTER 1

INTRODUCTION

The term composite refers to any multiphase, multicomponent material that exhibits a significant proportion of the properties of the constituent phases such that a better combination of properties is realized. According to this principle of combined actions, better property combinations are obtained by the judicious combination of two or more distinct materials (Callister 2005).

Nature uses composites for all her hard materials. For example, wood consists of strong and flexible cellulose fibers surrounded and held together by a stiffer material called lignin. Also, bone is a composite of collagen and other proteins and calcium phosphate salts.

A composite, in the present context, is a multiphase material that is artificially made, as opposed to one that occurs or forms naturally. Further, the constituent phases must be chemically dissimilar and separated by a distinct interface. Many composite materials are composed of just two phases, one is termed as the matrix, which is continuous and surrounds the other phase, often called the dispersed phase. In designing composite materials, scientists and engineers have ingeniously combined various metals, ceramics, and polymers to produce a new generation of extraordinary materials.

In this study, polymer nanocomposites consisting of an acrylic polymer as the matrix and nanofillers of different size, shape and chemical composition such as hydrotalcite (HT), sodium montmorillonite (MMT), carbon nanotubes (SWNT) and fullerenes (FUL) in carbon allotropes as the reinforcement media have been synthesized.

The composites have been characterized with scanning electron microscopy and wide angle X – ray diffraction to study the dispersion of the fillers in the polymer matrix. These polymer nanocomposites have also been characterized for mechanical, thermal and barrier properties and the results are reported in the subsequent chapters.

CHAPTER 2

POLYMER COMPOSITES WITH NANOFILLERS

2.1 General

World War 2 led to the explosive development of synthetic polymers such as nylon, acrylic, neoprene, polyethylene and many more polymers which found a wide range of applications in daily life due to their unique attributes such as ease of production, light weight and often ductile nature. However, polymers have lower modulus and strength as compared to metals and ceramics and hence had restricted applications. In order to improve their mechanical properties, polymers were reinforced with inclusions (fibers, whiskers, platelets, or particles), known as fillers. This addition of fillers into the polymer matrix to make composites was expected to result in material properties (mechanic, thermal stability and expansion, fire retardant, electrical and barrier properties) not achieved by either phase alone, and often lower cost. This practice improved polymer properties while maintaining their light weight and ductile nature; hence, the addition of fillers to polymers gained a lot of importance over the years.

Fillers are classified as inorganic (e.g. oxides, hydroxides, silicates, metals) and organic (e.g. carbon, natural and synthetic polymers) based on their chemical family. The fillers are also classified based on their shape and size or aspect ratio (ratio of length to diameter for a fiber or the ratio of diameter to thickness for platelets and flakes) as described in Table 2.1 (Xanthos 2005). Fillers may also be considered as continuous (long fibers or ribbons) or discontinuous (short fibers, flakes or particulates).

Table 2.1 Particle Morphology of Fillers

Shape	Aspect ratio
Cube	1
Sphere	1
Block	1 - 4
Plate	4 – 30
Flake	50 – 200++
Fiber	20 – 200++

Addition of these fillers to the polymer matrix needs to be done judiciously and economically. It is not possible to have one universal technique for making polymer composites due to the physical and chemical differences between each system, type of equipment available and different property modifications required for different types of applications. Melt mixing, *in situ* polymerization and solution mixing are the general approaches employed for making polymer composites. The melt mixing process involves heating a polymer and the filler mixture under shear, usually in an extruder, above the softening temperature of the polymer. *In situ* polymerization involves preparing a monomer solution or liquid monomer containing the fillers and then subjecting the mixture to polymerization. The solution method involves dissolutional polymers in common solvents and addition of the fillers followed by evaporation of the solvent in order to achieve the nanocomposite.

A prerequisite for effective reinforcement is optimal filler dispersion (agglomerate disintegration) and spatial distribution of the resulting particles in the polymer matrix. Figure 2.1 gives a schematic illustration of the difference between dispersion and distribution, giving examples of different extents for each (Schadler 2003). The real interest in polymer composites comes from the fillers, which provide value added properties not present in the neat matrix, without sacrificing the polymers

inherent processibility and mechanical properties. Parameters affecting the properties of polymer composites are:

1. The properties of the additives (inherent properties, size, shape).
2. Composition.
3. The interaction of components at the phase boundaries, i.e. the nature of the interphase.
4. The method of fabrication resulting in different microstructures and filler orientation.

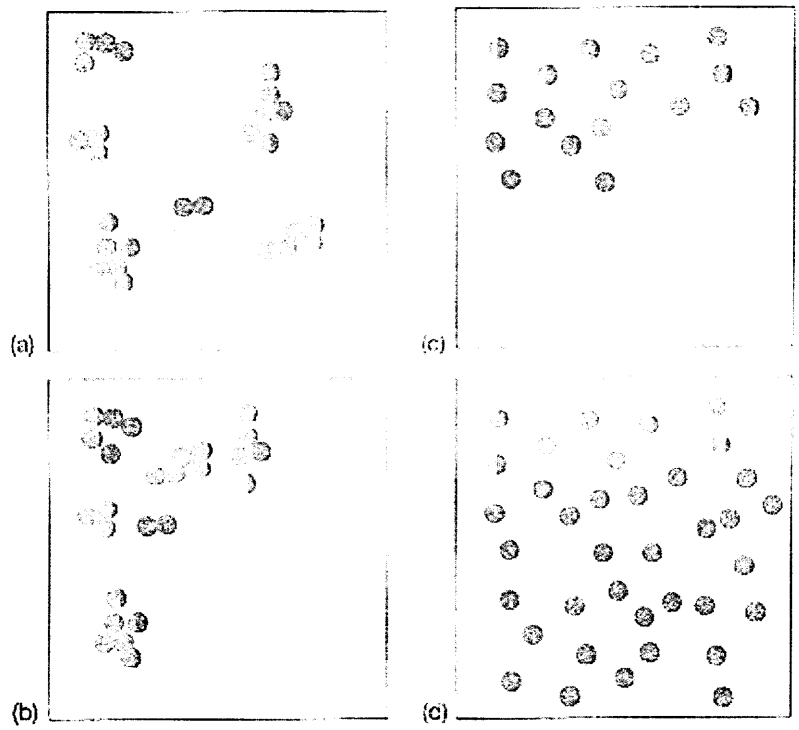

Figure 2.1 Schematic representation of distribution and dispersion of fillers; good distribution but poor dispersion (a), poor distribution and poor dispersion (b), poor distribution but good dispersion (c), and good distribution and good dispersion.

Traditionally, discontinuous composites were reinforced with micron sized or larger fillers. However, with the advances in technology and characterization techniques, scientists were able to see and study the properties of the nanosized particles (10^{-9} m) and they found that nanosized particles had far superior properties like increase in surface

area per unit volume and fewer defects, etc., when compared to their micron sized counterparts (Edelstein and Cammarata 1998).

As a result of improvement in properties and an increase in surface area with the nanosized particles, polymeric nanocomposites (involving fillers having at least one dimension in nanometers) have been an area of intense industrial and academic research, over the past 20 years, as they represent a radical alternative to conventional filled polymers. A review on the recent work on polymer matrix nanocomposites is presented by Jordan et al. (2005). Their review shows that even though no universal trend is present in polymer nanocomposites, better properties of composites are realized with nanofillers, which can lead to new applications. These nanofillers, irrespective of being either fibers or platelets, have extreme aspect ratios, which result in six interrelated characteristics distinguishing the resultant polymeric nanocomposites from classical filled systems (Vaia and Wagner 2004), at the same loading and extent of dispersion. They are:

1. Low percolation threshold (excluding spherical nanoparticle).
2. Particle-particle correlation (orientation and position) arising at low volume fractions (excluding spherical nanoparticle).
3. Extensive interfacial area per volume of particles.
4. Shorter distances between particles and
5. Comparable size scales among the rigid nanoparticle fillers, distance between particles, and the relaxation volume of polymer chains.

Based on the rules of mixtures, models for nanocomposites have been reported in order to describe the mechanical, barrier and other properties of the composites taking into consideration the type, shape and orientation of the fillers. Since the fillers employed in this study have been restricted to discontinuous fibers, flakes or platelets and

spherical particulates (additives that do not extend through the dimensions of the product and are dispersed throughout the continuous matrix), equations helpful in modeling properties using discontinuous fillers based on the above shapes of fillers, are provided. They have been summarized by Xanthos (2005) as shown below.

Modification of modulus and strength of polymers is one of the most compelling reasons for incorporating fillers into polymers. It is of utmost importance to select suitable filler taking into consideration the end application of the composite. For directional fillers with a certain aspect ratio (e.g. short fibers and flakes or plates) embedded in polymer matrices, the load is transferred from matrix to fibers or flakes by a shear stress and the ends of the fibers or flakes do not bare the load. An interpolation procedure applied by Halpin and Tsai has led to the general expression (Equation 2.1) for predicting modulus of composites containing short fibers and flakes or plates.

$$E_c / E_m = (1 + \xi\eta V_f) / (1 - \eta V_f) \text{ for } \xi = 2(\alpha) \qquad (2.1)$$

where,

E_c is the composite modulus,

E_m is the matrix modulus,

ξ is the adjustable parameter related to the aspect ratio 'α',

$\eta = (E_f / E_m - 1) / (E_f / E_m + \xi)$,

E_f is the filler modulus and

V_f is the volume fraction of the filler.

Equation 2.1 is valid for measurements of tensile modulus in longitudinal direction and it is modified based on measurements taken in transverse direction or at an angle to longitudinal direction. The stiffness behavior of particulate composites devised by

Kerner and further modified by Nielsen and co-workers is represented as shown in Equation 2.2.

$$E_c / E_m = (1 + ABV_f) / (1 - BXV_f) \quad (2.2)$$

where,

A,B and *X* are parameters related to geometry, moduli, volume fraction and packing fraction.

Models developed for strength of composites involving fibers and flakes take into account that the matrix deforms more than the filler at the filler ends and shear stresses are set up at the interface. Failure to the composite may occur either by filler fracture or bond fracture (filler pull out), depending on the filler aspect ratio. A critical fiber length L_{cr} and platelet diameter d_{cr}, defines the transition point between the two modes of failure for fibers and flakes or platelets, respectively. A critical aspect ratio, α_{cr} that determines the transition from fiber or platelet fracture to failure by debonding or shear failure of the matrix at lower stresses are given by Equations 2.3 and 2.4 for fibers and platelets, respectively.

$$\alpha_{cr} = \sigma_{fu} / 2\tau \quad (2.3)$$

$$\alpha_{cr} = \sigma_{fu} / \tau \quad (2.4)$$

where,

τ is the interface or matrix shear strength and σ_{fu} is the ultimate fiber or platelet strength.

The predictive equations used to describe the tensile strength of composites containing short fibers or platelets ignoring the effect of adjacent fibers or flakes, and the

presence of edges in irregularly shaped flakes are given in Table 2.2 (Xanthos 2005). Different equations are obtained for tensile strength measurements in different directions.

Table 2.2 Strength Equations for Short Fiber and Flake Composites

Tensile strength	Short fibers	Flakes
longitudinal; for fibers $L>L_{cr}$ or for platelet $\alpha_{cr}>\alpha$	$\sigma_c = \sigma_{fu}(1 - L_{cr}/2L)V_f + \sigma'_m(1 - V_f)$	$\sigma_c = \sigma_{fu}(1 - \alpha_{cr}/\alpha)V_f + \sigma'_m(1 - V_f)$
longitudinal; for fibers $L<L_{cr}$ or for platelet $\alpha_{cr}<\alpha$	$\sigma'_c = \tau L / dV_f + \sigma_{mu}(1 - V_f)$	$\sigma'_c = \tau\alpha / 2V_f + \sigma_{mu}(1 - V_f)$

σ_c is the composite strength; V_f is the volume fraction of the filler
σ'_m is the stress borne by the matrix when the fillers fail; σ_{mu} is the ultimate strength of the matrix;

Equation 2.5 is a general equation for the effect of particulate fillers on the tensile strength of polymer, a common modification of this equation by Nicolais and Narkis (Equation 2.6), and an additional equation proposed by Piggott and Leidner (Equation 2.7):

$$\sigma_c = \sigma_{mu}(1 - aV_f^b + cV_f^d) \tag{2.5}$$

$$\sigma_c = \sigma_{mu}(1 - 1.21V_f^{2/3}) \tag{2.6}$$

$$\sigma_c = \lambda\sigma_{mu} - KV_f \tag{2.7}$$

where,

a, b and c are constants depending on particle size and adhesion

λ is the stress concentration factor and

K is a constant depending on adhesion

Even though the models used for predicting the modulus and strength of composites in the transverse direction, or at an angle to the longitudinal direction have not been presented, it is important to summarize that the highest modulus in fiber composites is obtained in the longitudinal case, at an application angle of 0° and that the

lowest modulus is obtained in the transverse direction, i.e. in the extreme case of fiber misalignment, which is at an angle of 90°. Thus, in composites with fiber reinforcement, the composite modulus decreases rapidly with increasing orientation angle. However, in the case of composites with oriented platelets or flakes in a plane, isotropy may be achieved with modulus values higher than in the direction perpendicular to the flakes or platelets plane. Similar to the modulus in fiber composites, maximal strength for fiber composites is achieved in the longitudinal direction, with good adhesion, and at aspect ratio well above the critical value and the strength also decreases with increasing angle of application of stress. The strength of composites with platelets or flakes is isotropic in the plane of oriented platelets or flakes and much lower perpendicular to the platelet of flake plane axis.

In addition to mechanical property improvement, impermeable fillers also enhance the barrier property of composites (Matayabas and Turner 2000) by providing an increased resistance to transport of water vapor and other gases across the matrix. Filler particles, particularly platelets enhance the barrier property of polymers by providing a tortuous path for the transport of permeates, i.e. by offering obstruction to the passage of gases and other permeates through the matrix. A schematic illustration of the tortuous path for barrier enhancement is presented in Figure 2.2 (Matayabas and Turner 2000). Based on this, a tortuous path model was developed by Nielsen. As per this model, the barrier improvement is predicted to be a function of the volume fraction of fillers, V_f, and a function of the aspect ratio of the platey fillers, α, as shown in Equation 2.8.

$$P_c = (1 - V_f)P_m / (1 + \alpha V_f / 2) \quad (2.8)$$

where,

P_c represents the permeability of the resulting nanocomposite, and P_m represents the permeability of matrix polymer.

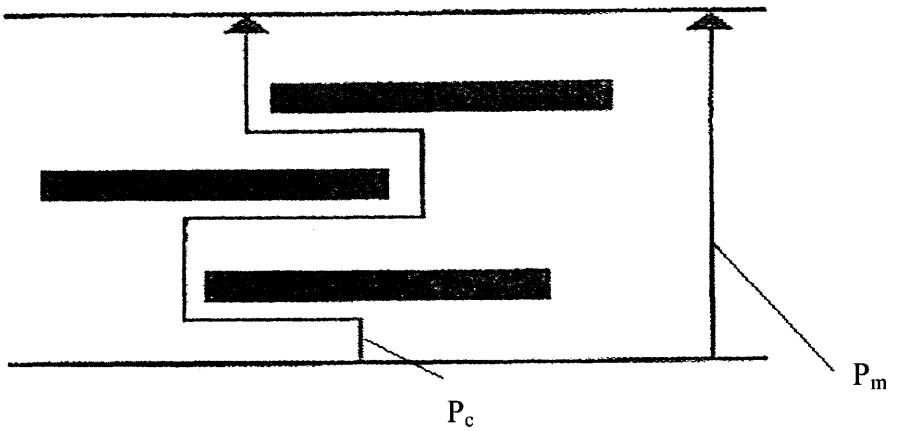

Figure 2.2 Illustration of Nielsen's tortuous path model for barrier enhancement of composite.

2.2 Composites with Nanoplatelets

Recently, much attention has been paid to polymer nanocomposites with clays as fillers having at least one dimension in the nanometer range since they give rise to a high degree of polymer – clay surface interaction which results in barrier and mechanical properties that are far superior to those of the neat polymer matrix (Pinnavaiaa and Beall 2000). With this idea, by using different clays and processing techniques, one can synthesize polymer-clay nanocomposites with compositional and structural variations that can be directed towards new applications.

The principle used in polymer composites with clays as reinforcements is to separate not only the clay aggregates, but also the individual silicate layers of clays in a polymer. By doing this, the excellent mechanical properties of the individual clay layers can function effectively, while the number of reinforcing components would also increase dramatically because each clay particle contains hundreds or thousands of layers. Thus, the preparation of polymer nanocomposite with clays requires extensive delamination of the layered clay structure and complete dispersion of the resulting platelets throughout the polymer matrix for effective reinforcement. *In situ* polymerization, solution mixing and melt mixing are the frequently used preparative methods for polymer – clay composites.

Depending up on the strength of the interfacial interaction between the polymer matrix and the layered clay, the Van Der Waals forces of attraction between the clay platelets, and the intensity of mechanical mixing, three different types of polymer – clay nanocomposite structures maybe obtained, as shown in Figure 2.3 (Carrado et al. 2000). They are: intercalated, semi-exfoliated and exfoliated structures. Figure 2.3 (a) represents the well ordered and stacked multilayer of clays that result from intercalated polymer chains within the clay layers. The semi-exfoliated structure is represented in Figure 2.3 (b), wherein the small stacks of polymer intercalated clay crystallites are well dispersed within a continuous polymer matrix, along with a few individual platelets of clays. Figure 2.3 (c) depicts the host layers that have lost their entire registry during processing and are well dispersed in a continuous polymer matrix; this is referred to as an exfoliated polymer – clay nanocomposite.

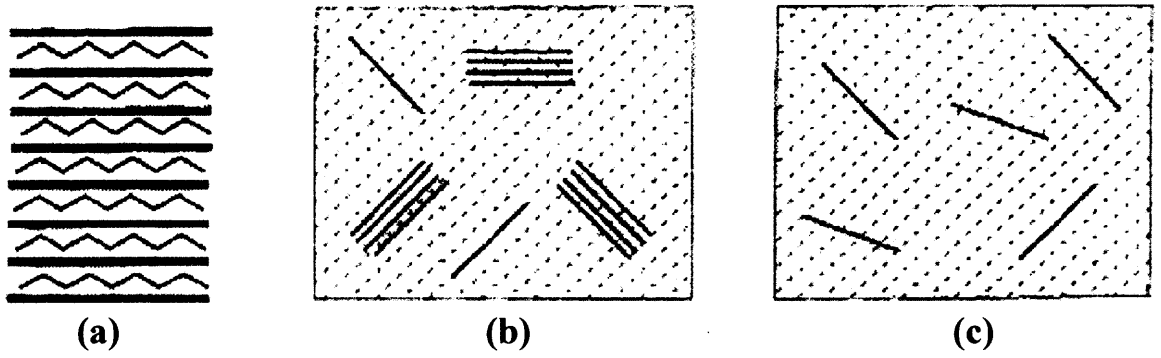

Figure 2.3 Schematic illustration of (a) intercalated: (b) semi-exfoliated and (c) exfoliated polymer-clay nanocomposites.

2.2.1 Montmorillonite Clays

Examples of different processing techniques for obtaining polymer – montmorillonite composites are given below.

Bulk polymerization of ε-caprolactone was carried out at 170°C in the presence of water and hydrated synthetic montmorillonite, with additional catalysts in order to study the structure of poly(ε-caprolactone)/synthetic montmorillonite composites by Kiernowski et al. (2004). Their studies showed that while the polymerization rate was enhanced in the presence of montmorillonite, the molecular weight of the final polymer is lowered. Wide angle X-ray scattering studies of the composites showed that intercalated structure was obtained with synthetic montmorillonite after the polymerization of ε-caprolactone.

Solution mixing was employed by Chang et al. (2003) in order to compare the properties of nanocomposites made from organo montmorillonite (OMMT) and organo mica with poly(lactic acid). XRD and TEM results showed that for the OMMT composite, the polymer chains were intercalated within the clay galaries and that for O-mica composites, there were partially delaminated sheets in the matrix and regions where

a regular stacking of sheets (semi – exfoliated structure) were maintained with a layer of polymer between the sheets. Mechanical property characterization showed that the introduction of organo clay increases the elongation at break, the ultimate tensile strength of composites also increases with loading up to a critical wt% loading. Their studies also showed that the initial modulus increases with OMMT up to 4 wt% and up to 8 wt% for O–mica. However, thermal studies surprisingly showed that with 4 wt% loading of organo clay, the decomposition of composites occurs at a lower temperature when compared to that of the unfilled polymer matrix.

Melt processing technique was employed by Jiang et al. (2005) to make Nylon 6/OMMT composites, in order to study the barrier property of the composite. Their experiments showed that the reinforcement of Nylon 6 with OMMT resulted in improved resistance to solvent permeation due to the increase in crystallinity and the decrease in crystalline size of nylon 6 with optimum value of clay loading along with the more tortuous path encountered by the diffusing molecule due to the presence of clay.

Tensile properties of nanocomposites with organo montmorillonite and high density polyethylene (HDPE) were studied by Osman et al. (2005). Their study showed that even partial exfoliation of OMMT would affect the mechanical properties of nanocomposite. Their results showed that enhanced exfoliation would not only slightly increase the elastic modulus and yield stress, but at the same time it would also decrease the yield strain and stress at break. Furthermore, they also showed that with increasing filler loading at low loading levels, while the elastic modulus of the composites would increase, all other tensile properties would decrease.

2.2.2 Hydrotalcite

A melt mixing process was employed by Velasco et al. (2005) for preparing nanocomposites from polypropylene homopolymer (PP) and high density polyethylene (HDPE), with unmodified magnesium aluminum type of layered double hydroxides containing carbonate ions (LDH) and an organic modified LDH(DS). Studies showed that while the Young's modulus and tensile strength increased for nanocomposites with PP the mechanical properties were practically unaffected by the presence of fillers for HDPE nancomposites. Thermal characteristics from DSC showed that the crystallization temperature was significantly affected with the presence of LDH(DS) in PP. Nanocomposites with HDPE showed little or no changes in thermal studies. Their studies also showed that the flame behavior of both polymers were modified by the presence of nanofillers.

Wagenknecht and Coasta (2005) studied the rheological , thermal and mechanical properties of composites of polyethylene with magnesium hydroxide nanoplatelets (layered double hydroxide based on Mg and Al). Their thermal studies showed that there was a significant improvement in thermal stability with 10phr loading of the filler. Mechanical studies showed that while the modulus and elongation at break increased, the tensile strength was reduced in the presence of the filler.

2.3 Composites with Carbon Allotropes

2.3.1 Carbon Nanotubes

There has been a tremendous interest in carbon nanotubes ever since their discovery by Iijima (1991), in large part because they possess unique structural and electrical properties along with excellent mechanical properties. Single walled (SWNT) and multi walled (MWNT) are the two general classifications of carbon nanotubes. In particular, considerable interest surrounds the concept of nanocomposites based on carbon nanotubes as a means to capitalize on their extraordinary properties on a macroscopic scale. It is believed that polymer carbon nanotube composites will have a significant impact on emerging advanced products ranging from aerospace, automotive and proton exchange membrane fuel parts, to surgical implants and to components of nanoelectronics (Iqbal et al. 2005).

As mentioned before, several processing methods are available for producing polymer carbon nanotube composites based on either thermoplastics or thermosets, such as solution processing, in-situ polymerization and melt mixing. Even though these techniques are inherently different, all of them attempt to address the issues described before for nanosized fillers, in order to achieve the effective utilization of nanotubes through alignment, uniform dispersion in the polymer matrix and good interfacial bonding, the latter affecting the load transfer across the polymer – nanotube interface.

Carbon nanotubes, owing to their small size, tend to remain agglomerated in the polymer matrix and uniform dispersion is not easily achieved. This is one of the most significant problems in making composites and this problem is further aggravated with the use of water based polymers, since carbon nanotubes are hydrophobic in nature.

However, in order to achieve good reinforcement in a composite, it is critical to have uniform dispersion within the matrix. Sodium Dodecyl Sulfate was used as an effective dispersing agent for carbon nanotubes in water by Jiang et al. (2003). Other investigators have used other methods in order to achieve good dispersion in the polymer matrix such as: a solution evaporation method with high energy sonication (Qian et al. 2000), surfactant assisted processing through formation of a colloidal intermediate (Shaffer and Windle 1999) or covalent functionalization of nanotubes with polymer matrix (Bratcher et al. 2001), in order to achieve good dispersion in the polymer matrix.

Literature examples on preparation and characterization of carbon nanotube composites are given below.

In situ polymerization of ε-caprolactam in the presence of pristine and carboxylated multiwall carbon nanotubes was used by Zhao et al. (2005) to prepare Polyamide 6/carbon nanotube composites. They ultrasonically dispersed CNT's in a mixture of ε-caprolactam and water to form a homogeneous polymerizable master solution. Then, additional ε-caprolactam was added to obtain composites using typical Polyamide 6 hydrolytic polymerization conditions. Viscosity measurements showed that low loadings of 5wt% of CNT's have minimal effect on molecular weight. Mechanical studies on the composite showed that while the presence of CNT's in Polyamide 6 has little effect on the yield strength, they improved the tensile strength marginally and decreased the elongation at break. CNT's also increased the storage modulus of the composites slightly. Their studies also show that while the CNT's have no effect on the melting temperature of the composites, they slightly increased the crystallization and glass transition temperature. Using a similar technique of *in situ* polymerization, Park et

al. (2002) achieved uniform dispersion of single wall carbon nanotubes bundles in the polymer matrix which resulted in a sharp increase in conductivity at a low loading of 0.1 vol%. Their dynamic mechanical analysis showed a 60% improvement in the modulus at 1.0 vol% of SWNT loading. The thermal conductivity of the composite was also enhanced with the addition of SWNT's.

Different compounding methods such as ball milling, high shear mixing in melt and extrusion using twin screw extruder were employed by Ma et al. (2003) to make polyester/carbon nanofiber composites. These composite resins were further melt spun into fibers using conventional fiber spinning conditions. Mechanical property studies revealed that even though the tensile strength and modulus of the composite did not improve significantly, the torsion moduli of the composite fibers were considerably higher than the control PET fiber. Their study also revealed that there may be an optimum fiber length which provides for effective reinforcement and easy processing.

Thostenson and Chou (2002) dispersed 5 wt% MWNT in a polystyrene matrix with the help of a twin screw extruder. Dispersion of nanotubes was followed by extruding the polymer melt through a rectangular die and drawing the film prior to cooling or by pressing a film using a hydraulic press in order to obtain aligned or randomly oriented nanocomposite films, respectively. Characterization of films revealed that addition of nanotubes increased the tensile modulus, yield strength and ultimate strength of the polymer film. They also showed that with an aligned nanotube composite, the elastic modulus was 5 times greater than that for a randomly oriented nanocomposite. Similarly, Haggenmueller et al. (2000) also showed that the electrical and mechanical

properties of poly(methyl methacrylate) containing SWNT improved with the alignment and wt% of carbon nanotubes (up to 8 wt% purified soot).

Space durable polymer (polyimide) nanocomposite films using carbon nanotubes were synthesized by Delozier et al. (2005), using a solution technique. Their studies revealed that the prepared films exhibited electrical conductivity in the range, sufficient to dissipate static charge. But, the inclusion of SWNTs in the polymer had a negligible effect upon the T_g and little or no effect on the tensile properties.

According to Kymakis et al. (2002), single wall nanotubes were dispersed in chloroform or toluene with the help of a high power ultrasonic probe. Poly(3-octylthiophene) was also dissolved in chloroform and toluene. The above were mixed in appropriate quantities and the final solution was briefly sonicated. They reported that doping of a conducting polymer with nanotubes to form a composite increased the conductivity of the composite by five orders of magnitude.

Carbon nanotube/PMMA composites were fabricated by melt blending and compression using a hot press by Jin et. al. (2001); their method did not cause any damage to the nanotubes. TGA studies of the PMMA and the composites under nitrogen atmosphere showed that with the incorporation of the MWNT into the PMMA, the onset of degradation occurs at a higher temperature. Hence, the MWNT provide a stabilizing effect on the PMMA. Dynamic mechanical analysis showed that the storage modulus of PMMA was increased with the help of nanotubes, this effect was even more pronounced at higher temperatures. DMA analysis also showed that the glass transition temperature of the composite increased in the presence of nanotubes.

2.3.2 Fullerenes

The influence of fullerene additives on thermal behavior and thermodegradation of poly-n-alkyl acrylates, from butyl to heptyl, and of corresponding polymethacrylates was studied by Zuev et al. (2005) using thermogravimetry in dynamical conditions and pyrolysis/gas chromatography in isothermal conditions at 400 – 650°C. Their studies showed that fullerene modifies the degradation products distribution, suppressing the decomposition reaction with radical pathway and shifting the thermodegradation to non radical side-chain reactions. Their studies also showed that fullerene acts as an effective stabilizer increasing the thermostability of the polymers. However, the increase of the temperature to maximum weight loss is noticeably higher for poly-n-alkyl methacrylates.

Literature search on examples for preparation and characterization of fullerene composites did not result in the identification of other papers, related to this study.

CHAPTER 3

EXPERIMENTAL

3.1 Materials

3.1.1 Acrylic Paint Polymer

The polymer used to prepare the composite was a water based acrylic protective finish (Minwax® Polycrylic®, Minwax Co., NJ) drying to a clear flexible film. According to the manufacturer's safety data sheet, the paint has a specific gravity of 1.03 and contains 71% of volatile content by volume. In addition to water, and other chemicals which are exempt from listing on the TSCA inventory, solvents used in the paint include propanol, 1(or 2)-(2-methoxymethylethoxy); (2-methoxymethylethoxypropanol), 1-(-butoxy-1-methylethoxy)-2-propanol; (1-(2-butoxymethylethoxy)-propanol), ethylene glycol, decylpoly(ethyleneoxy)ethanol, 1-methyl-2-pyrrolidinone. The pH of the paint as reported on the MSDS is 8.1.

3.1.2 Hydrotalcite

Hydrotalcite is a natural mineral with a white color and pearl like luster. Natural hydrotalcite is a hydrated magnesium-, aluminum-, and carbonate-containing mineral with a layered structure. Hydrotalcite can also be made synthetically in order to have different compositions by replacing the carbonate anions with other anions (Patel 2005). The composites involving hydrotalcite were formed by using uncoated hydrotalcite (HT) (trade name CLC-120), obtained from Doobon Yuhwa Co, Ltd, S. Korea. The hydrotalcite was obtained in the form of white powder, with a reported average particle size of 0.4-0.5μm and having a molar ratio for MgO/Al_2O_3 of 4.0-5.0. A typical

chemical structure of hydrotalcite is $Mg_4Al_2(OH)_{12}CO_3.3H_2O$. The three-dimensional, double layered structure of a typical hydrotalcite consisting of magnesium and aluminum hydroxide octahedrons, interconnected through their edges can be seen in Figure 3.1 (Patel 2005). Results of EDX for the hydrotalcite sample is given in Appendix A.1 and particle morphology showing platelets of low aspect ratio are shown in Figure 4.3.

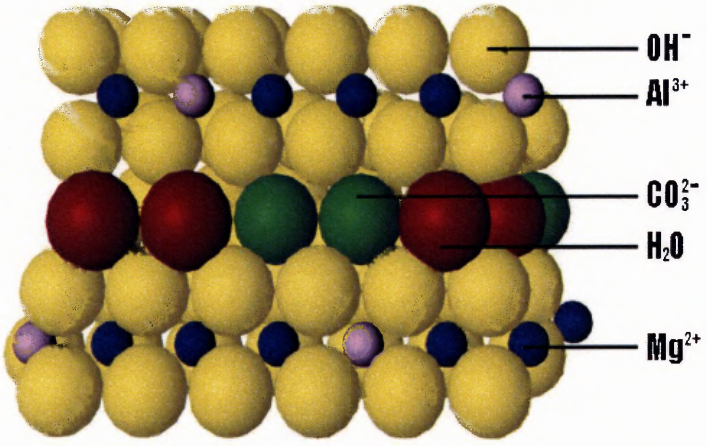

Figure 3.1 Molecular structure of hydrotalcite.

3.1.3 Sodium Montmorillonite

Sodium Montmorillonite, or natural sodium bentonite is a rock composed essentially of crystalline clay like mineral, formed by devitrification, and the accompanying chemical alteration of a glassy igneous material, usually a turf or volcanic ash. This clay belongs to the family of smectite group of clay minerals, which have excellent intercalation abilities. Sodium montmorillonite is composed of hydrated aluminum silicate and as the name suggests occurs with sodium as the predominant exchange cation. The composites

(Minami 2002). In size, SWNT's are close to fullerene molecules and have a single layer cylinder extending from end to end. They possess good uniformity in diameter of 1-2nm.

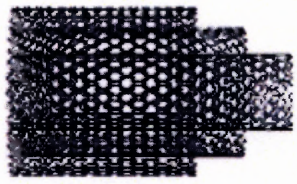

Figure 3.3 Schematic picture of multi walled carbon nanotube.

Figure 3.4 Schematic picture of single walled carbon nanotube.

The perfect alignment of the lattice along the tube axis and the closed topology endow nanotubes with in-plane properties of graphite, such as high conductivity, excellent strength and stiffness, chemical specifity, inert toughness and good electronic properties. Carbon nanotubes have a very broad range of these properties depending on their diameter, length and chirality or twist. The measured and theoretical properties of both SWNT and MWNT are shown in Table 3.1 (Schadler 2003).

Table 3.1 Properties of Carbon Nanotubes

Property	Nanotubes
Specific gravity	0.8-1.8 $g.cc^{-1}$ (theoretical)
Elastic modulus	~ 1 TPa for SWNT ~0.3-1 TPa for MWNT
Strength	50-500 GPa for SWNT 10-60 GPa for MWNT
Resistivity	~5-50 μ- Ω-cm
Thermal conductivity	3000 $Wm^{-1}k^{-1}$ (theoretical)
Thermal expansion	Negligible (theoretical)
Oxidation in air	700 C

The single walled carbon nanotube (SWNT) sample used in the preparation of composites in this work was kindly provided by Prof. Roman Dubrovsky (Department of Mechanical Engineering, NJIT). Soot containing SWNT's was produced by the arc discharge method. The arc is generated between two graphite electrodes in a reactor under helium atmosphere. A mixture of 1% Y and 4% Ni was used as a catalyst. The resulting soot containing SWNT's is removed from the reactor and is normally subjected to purification. In the present study, the sample used contains up to 15 wt% SWNT's in carbon soot. The EDX results of the samples used in the preparation of the composites is given in Appendix A.3. Particle morphology indicating the presence of some very high aspect ratio flexible fibers is shown in Figure 4.9.

3.1.5 Fullerenes

Fullerenes are similar to graphite in structure, since they tend to form by rolling up of graphite sheets and adding pentagons to achieve curvature. The smallest fullerene, which is one of the most stable forms of carbon atom cluster is also known as buckminsterfullerene and it contains 60 carbon atoms bonded in the near spherical configuration, as shown below in Figure 3.5 (Yarris).

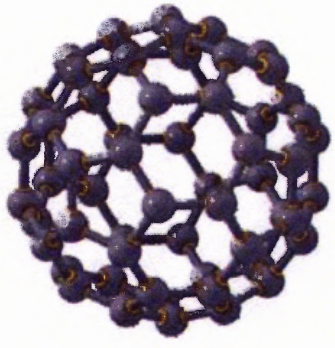

Figure 3.5 Buckminsterfullerene image.

In a C_{60} molecule, each carbon atom is equivalent to all others (i.e., they all have the same number of neighbors, bonded at the same relative angles). It has a truncated icosahedron shell structure, with 20 hexagons and 12 pentagons attached in a manner that no 2 pentagons are adjacent to each other. A C_{60} molecule or "bucky ball" is about 0.7nm in diameter.

The fullerene (FUL) sample used in the preparation of the composites in this work was kindly provided by Prof. Roman Dubrovsky (Department of Mechanical Engineering, NJIT). The method used in the production of fullerenes has been reported by Dubrovsky and Bezmelnitsyn (2004) as a novel technique based on the arc discharge method. They employed the gas outflow approach using a modified cathode, with a longitudinal inner channel to inject helium as a buffer gas to the graphite electrode gap between the cathode and the anode. Their idea was that the radial gas outflow will evacuate the rapidly produced vapor from the hot plasma zone to the reactor and increase the fullerene yield % in the carbon soot at an optimum level of dilution by the buffer gas. They also showed that with increasing anode surface temperature, above a certain critical temperature the efficiency of fullerene formation is diminished inspite of increasing the amount of vapor. Accordingly, in order to obtain good quality of carbon vapor suitable for fullerene formation it is necessary to maintain a hot anode surface whose temperature is equal to or less than the critical temperature. Any increase in temperature above this critical value will result in the production of soot but not fullerenes. The authors used their findings to obtain a maximum yield of vaporized graphite under optimum outflow arc discharge conditions and an optimum temperature of the surface of anode. In the present study, the sample used contains up to 10 wt% fullerenes in carbon soot. The

EDX result of the fullerene sample used in the preparation of the composites is given in Appendix A.4. Particle morphology indicating the presence of particulates with an aspect ratio close to unity is shown in Figure 4.10.

3.2 Processing of Composites

The processing method employed in the synthesis of polymer nanocomposites was a mixture of solution mixing and solvent casting. Nanofillers (5 or 10 wt% based on paint solid contents) were dispersed in the acrylic polymer paint by sonication for 2 hours (temperature at the end of sonication was 35°C), and subsequently by a mechanical shear mixer for 20 minutes at room temperature. In order to remove the bubbles formed during mixing, the mixture was further subjected to 6 hours of magnetic stirring at room temperature. Paint films (composites) containing the nanofillers were drawn down to about 1 mm thickness, on Teflon sheets with a BYK Gardner knife coating device. 4-5 ml of 1 wt% dioctyl sulfosuccinate sodium salt (Sigma Aldrich (CAS# 577-11-7) solution in distilled water, was used to facilitate the wetting of the hydrophobic fullerene and single walled nanotube samples with paint. Paint films of acrylic polymer without the nanofillers were also prepared, as the reference composite used in the comparison of properties of various composites. All the films were dried at room temperature for 5 days, followed by drying at 50°C under vacuum for 24 hours. The average final thickness of the films at the end of drying was varying from 0.098 to 0.58 mm. The acrylic polymer film was transparent after drying. While the films with hydrotalcite and montmorillonite fillers were transparent to translucent due to the dispersion of the fillers, the films with nanotubes and fullerenes as fillers were opaque and black in color.

3.3 Testing and Characterization

3.3.1 Scanning Electron Microscopy (SEM)

A LEO 1530 emission scanning electron microscope was used for SEM observation. The crossection samples were sputter coated with carbon prior to their observation. However, no sputtering was required to view the nanofillers alone. The surface atomic composition of the nanofillers was examined by energy dispersive X-ray analysis.

3.3.2 Wide Angle X-Ray Diffraction (WAXRD)

The structure of nanofillers and composites was determined by X-ray diffraction (XRD), using a Philips PW3040 diffractometer (Cu Kα radiation λ=1.5406Å, generator voltage = 45 kV, current = 40 μA) in order to determine the effects of polymer on inter planar distance. All the specimens were scanned in 2θ ranges from 1°– 50° at a rate of 1°/min. Measurements were recorded for every 0.03°. Plots of intensity versus 2θ° were plotted. Changes in the interlayer spacing 'd' of fillers after dispersion in the polymer matrix were measured using the Bragg's law of diffraction (Equation 4.1).

$$D = n\lambda / 2\sin\theta \qquad (3.1)$$

where,

n is an integer,

λ is the wavelength of the incident X-ray beam in A˙ and

θ is the angle of incidence in degrees.

3.3.3 Mechanical Properties

3.3.3.1 Tensile Properties. The tensile strength, elongation at break and the 2% secant modulus of the composites were measured using a Tinius Olsen LoCap universal testing machine, using the ASTM D 882 procedure. While the initial gap separation was 2.54cm for all measurements, the crosshead speed of 25.4cm/min was used for strength and elongation measurements and the crosshead speed of 0.254cm/min was used for the secant modulus measurements at room temperature. Test specimens of 1.27cm width, 8cm length and 0.2-0.4mm thickness were machined out from the composites for the above measurements. Multiple measurements were taken for each composite in order to estimate the precision of the results.

3.3.3.2 Dynamic Mechanical Analysis (DMA). DMA was performed under nitrogen atmosphere using a DMTA 4 (Rheometric Scientific) at a heating rate of 5.0°C/min. The dynamic temperature ramp test was done at a vibration frequency of 1Hz, with the temperature range from -40°C to 150°C at a strain of 0.05%. The specimens used for measuring storage modulus and tanδ were rectangular in shape and had approximate dimensions of 16mm*4mm*0.3mm.

3.3.4 Thermal Analysis

3.3.4.1 Differential Scanning Calorimetry (DSC). Information on the glass trans -ition temperatures of the polymer and the composites were got by using TA Instruments' QA 100 differential scanning calorimeter. All samples were scanned at heating and cooling rates of 15°C/min, from - 60°C to 200°C in a nitrogen atmosphere.

3.3.3.2 Thermogravimetric Analysis (TGA). The thermal stability of nanofillers, polymer and composites were studied using TA Instruments' QA 50 thermogravimetric analyzer. Tests were carried out using a ramp from room temperature to 500°C, with a scan rate of 10°C/min in nitrogen atmosphere.

3.3.5 Barrier Property

The permeability test of the composites conformed to the ASTM Standard Test Methods for Water Vapor Transmission of Materials (ASTM E-96). Specifically, the water method was used for testing the composite samples. This test evaluates the amount of water that permeates through the material being tested. A cup was filled with distilled water leaving a small gap (18 to 6 mm) of air space between the specimen and the water. The cup was then sealed to prevent any vapor loss from locations other than the test sample. Apart from noting down the initial weight of the cup assembly, the cup assembly was periodically weighed over time until linearity was achieved in a plot of weight change versus time. Water vapor transmission rate (WVTR) was calculated using Equation 3.6.

$$WVTR = (G/t)/A \tag{3.2}$$

where,

G = weight change from the straight line, g; t = time, hr; G/t = slope of the straight line, g/hr; A = test area (cup mouth area), m^2, and WVTR = rate of water vapor transmission, $g/hr.m^2$.

CHAPTER 4

RESULTS AND DISCUSSION

This section will provide results from the experiments carried out to elucidate the effects of the different fillers on the properties of the polymer nanocomposites. Results for the acrylic polymer alone will also be reported in order to compare the properties of the polymer with those of the composites.

4.1 Scanning Electron Microscopy of Fillers and Composites

Scanning electron microscopy was used to qualitatively characterize the distribution of nanofillers, along with their orientation within the acrylic polymer. Cross section images of the cryofractured and tensile fractured composites were studied. The cross sections of composites were subjected to carbon sputtering in order to avoid charging. SEM images of the nanofillers prior to their incorporation in the polymeric matrix were also taken for comparison.

Figure 4.1 (a), (b) and (c); show selected images of cryofractured PHT – 5 (polymer/5 wt% hydrotalcite), while Figure 4.2 (a), (b) and (c); present the selected tensile fractured sections of PHT - 5. Images of as used HT platelets of low aspect ratio and irregular particles are also shown in Figure 4.3 (a), (b) and (c), for comparison.

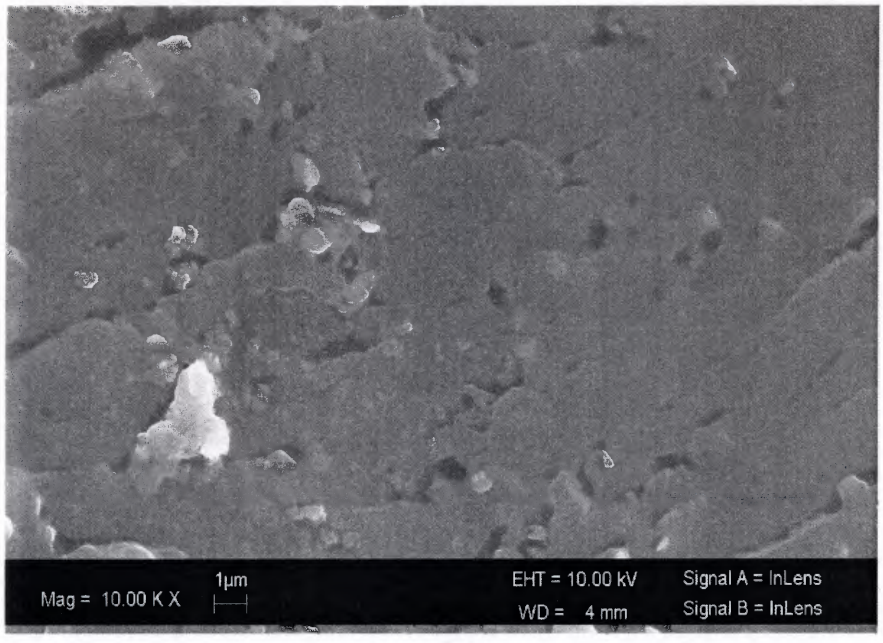

(a)

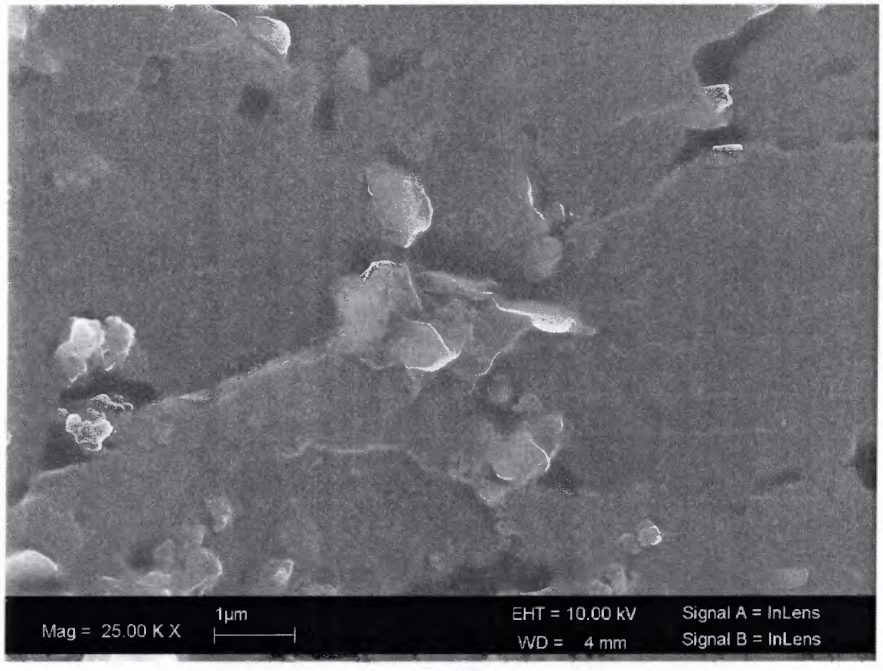

(b)

Figure 4.1 (a), (b) and (c) SEM images of cryofractured crossection of PHT – 5.

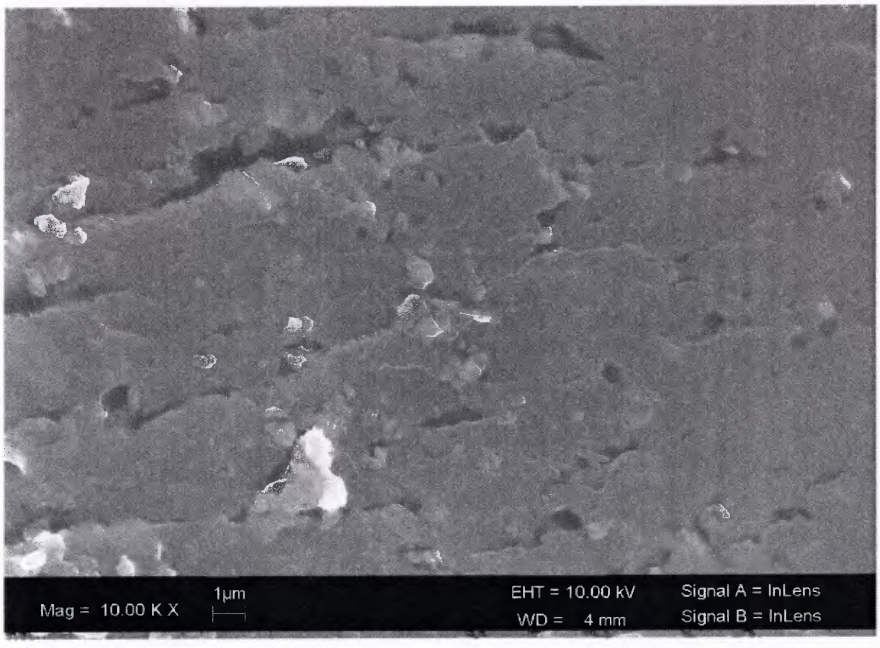

(c)

Figure 4.1 (a), (b) and (c) SEM images of cryofractured crossection of PHT – 5. (Continued)

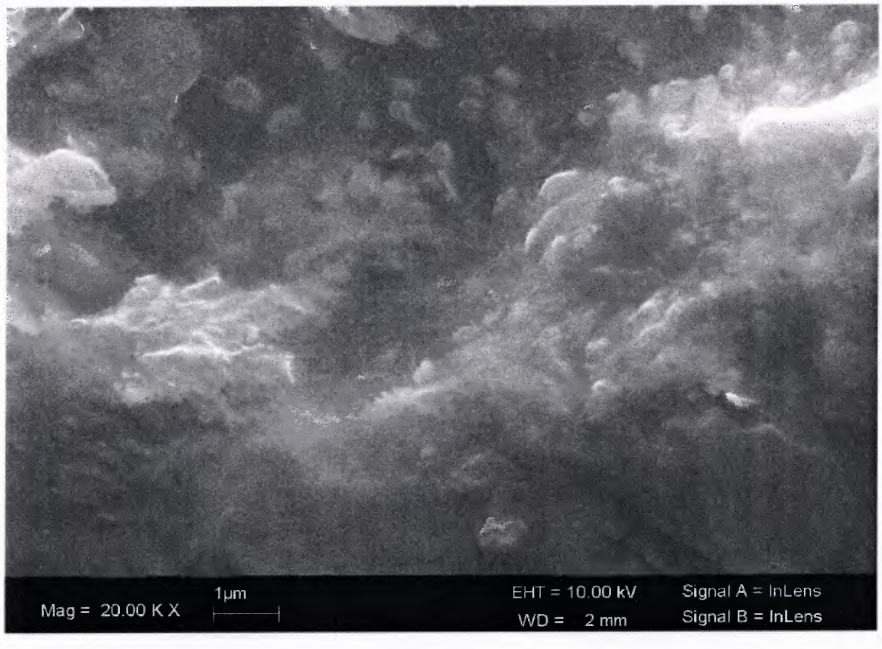

(a)

Figure 4.2 (a), (b) and (c) SEM images of tensile fractured crossection of PHT – 5.

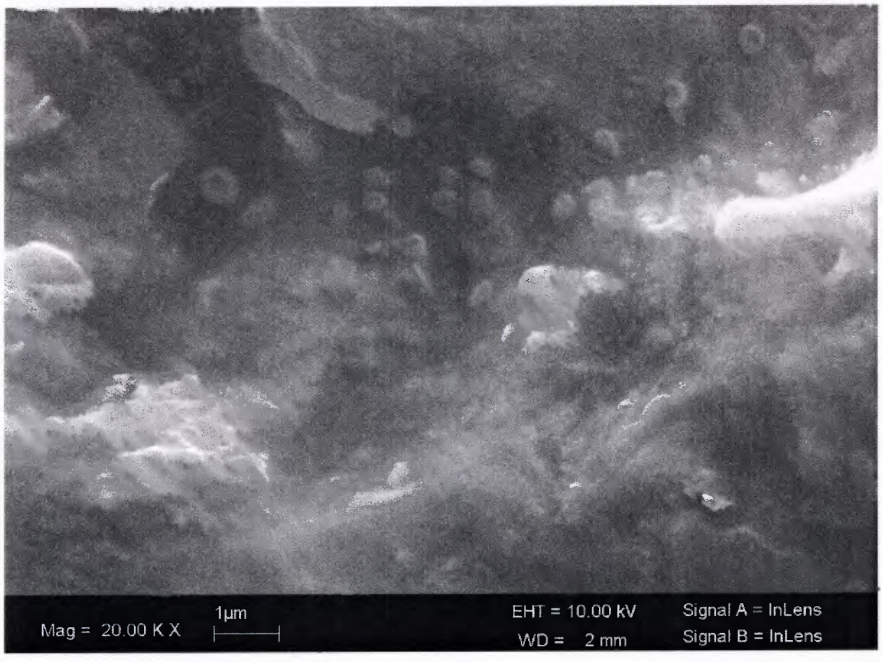

(b)

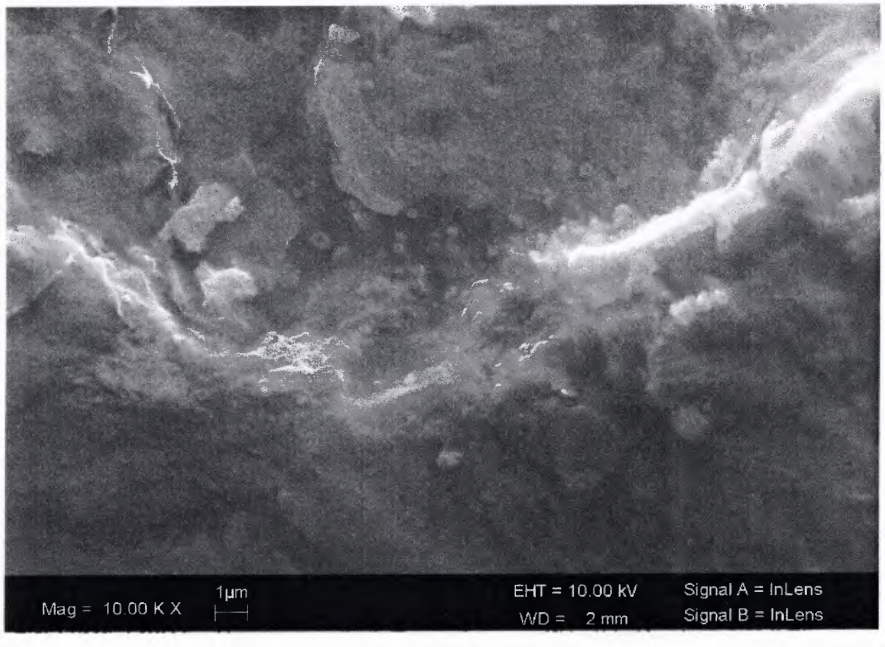

(c)

Figure 4.2 (a), (b) and (c) SEM images of tensile fractured crossection of PHT – 5. (Continued)

Figures 4.1 and 4.2 not only show good distribution of the HT filler in the acrylic polymer (PACR) but also show poor adhesion to the matrix. These images also show that there is no alignment of the HT filler platelets in the plane of draw down.

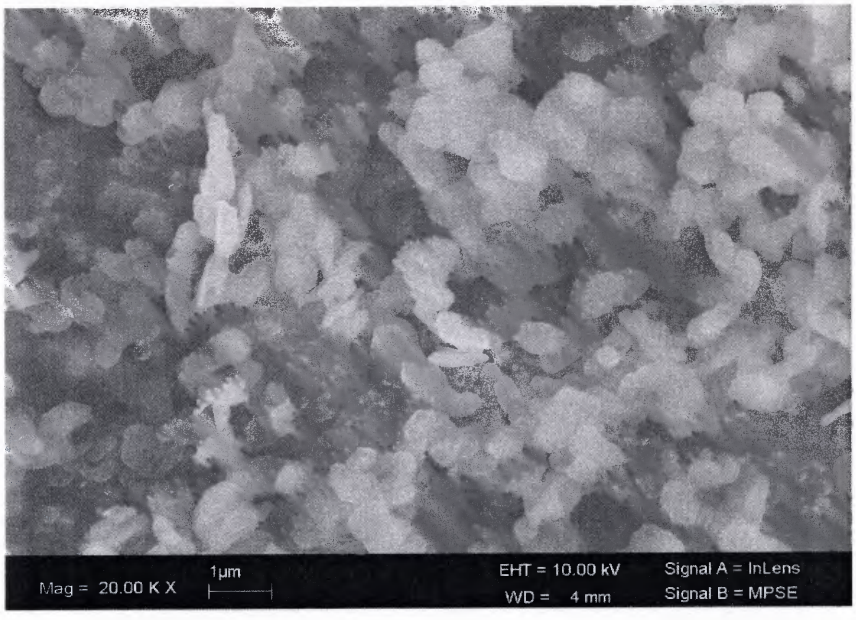

(a)

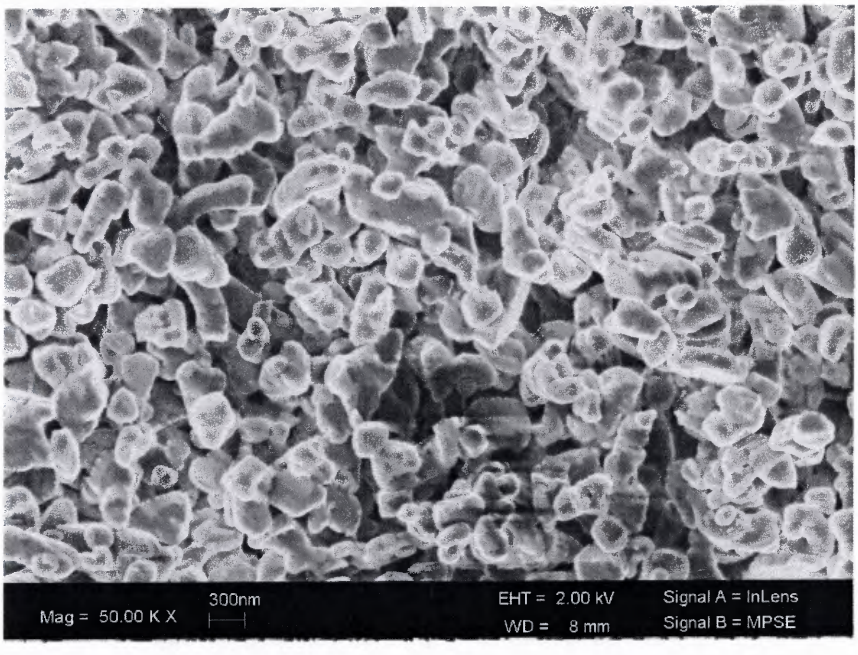

(b)

Figure 4.3 (a), (b) and (c) SEM images of as used HT.

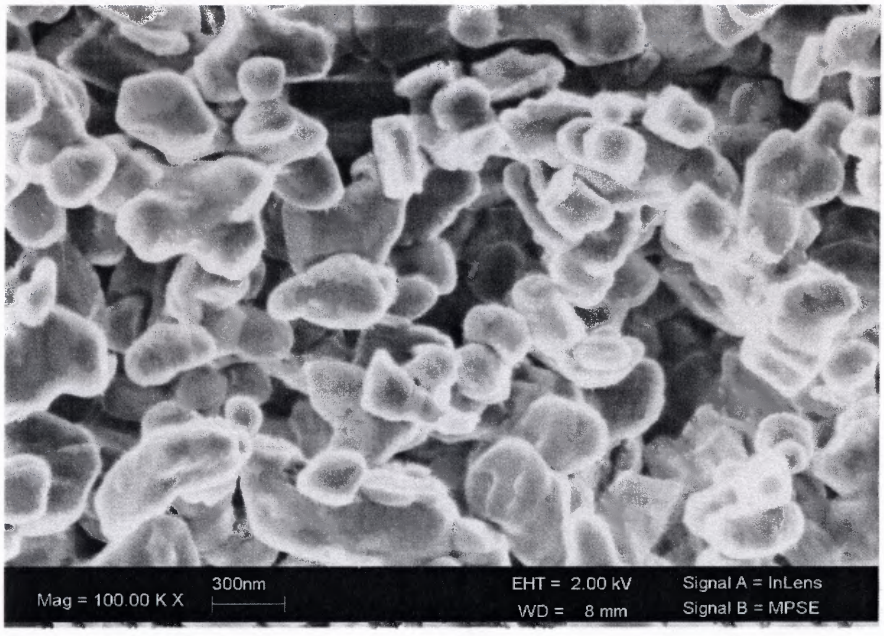

(c)

Figure 4.3 (a), (b) and (c) SEM images of as used HT. (Continued)

Selected SEM image of the cryofractured PMMT – 5 (polymer/5 wt% sodium montmorillonite) composite is shown in Figure 4.4; the selected tensile fractured images are shown in Figure 4.5 (a) and (b). SEM images of the as used MMT aggregates prior to dispersion are also shown in Figure 4.6 (a), (b) and (c). These images show good distribution of intercalated MMT platelets in the acrylic polymer and they also show that there is no alignment of the platelets in the plane of draw down. Adhesion also appears to be poor.

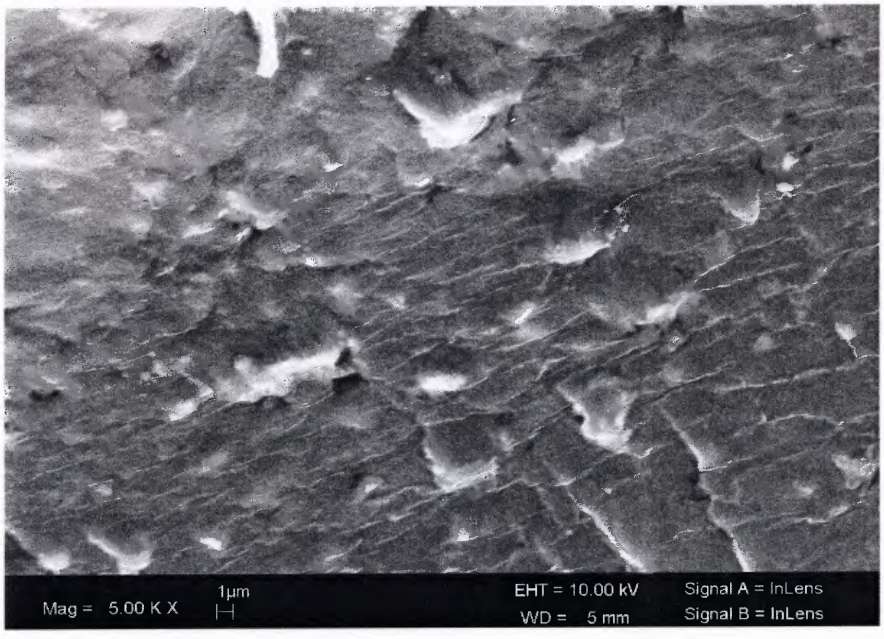

Figure 4.4 SEM image of cryofractured crossection of PMMT – 5.

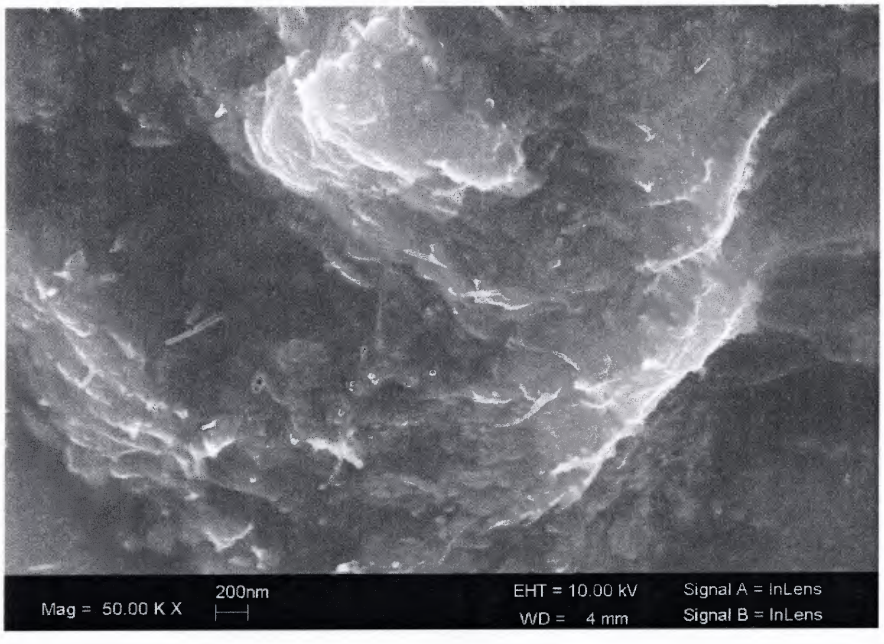

(a)

Figure 4.5 (a) and (b) SEM images of tensile fractured crossection of PMMT – 5.

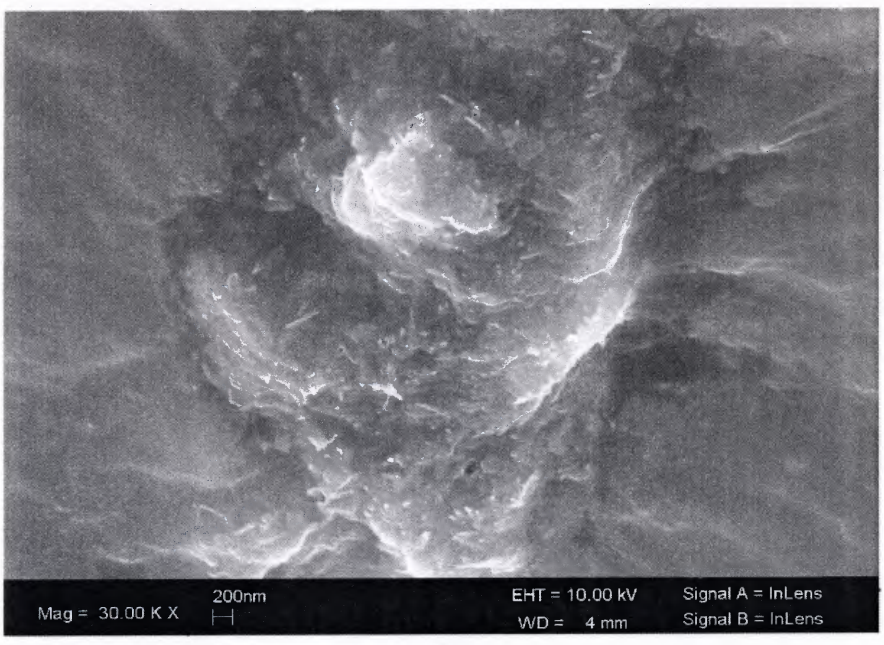

(b)

Figure 4.5 (a) and (b) SEM images of tensile fractured crossection of PMMT – 5. (Continued)

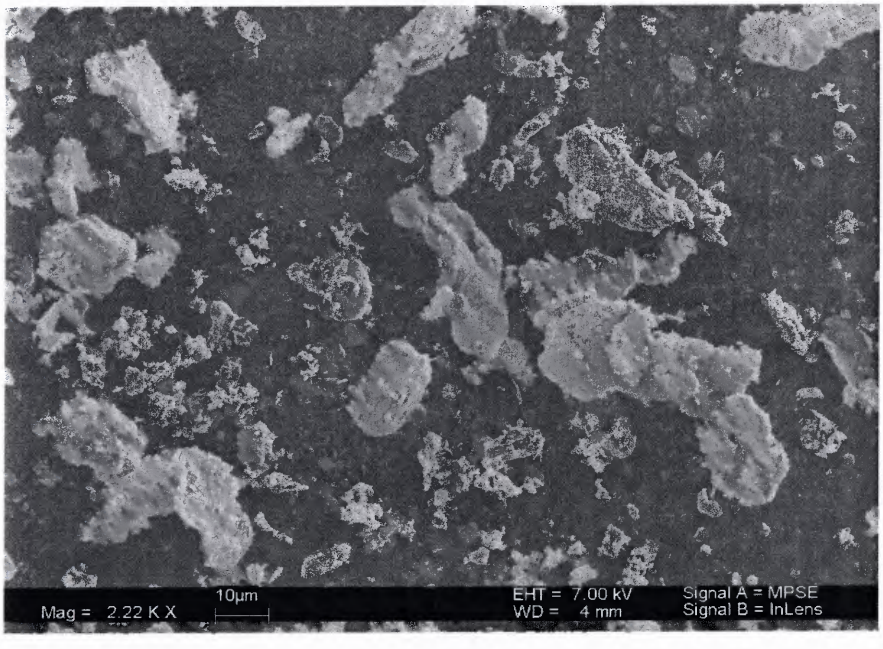

(a)

Figure 4.6 (a), (b) and (c) SEM images of as used MMT.

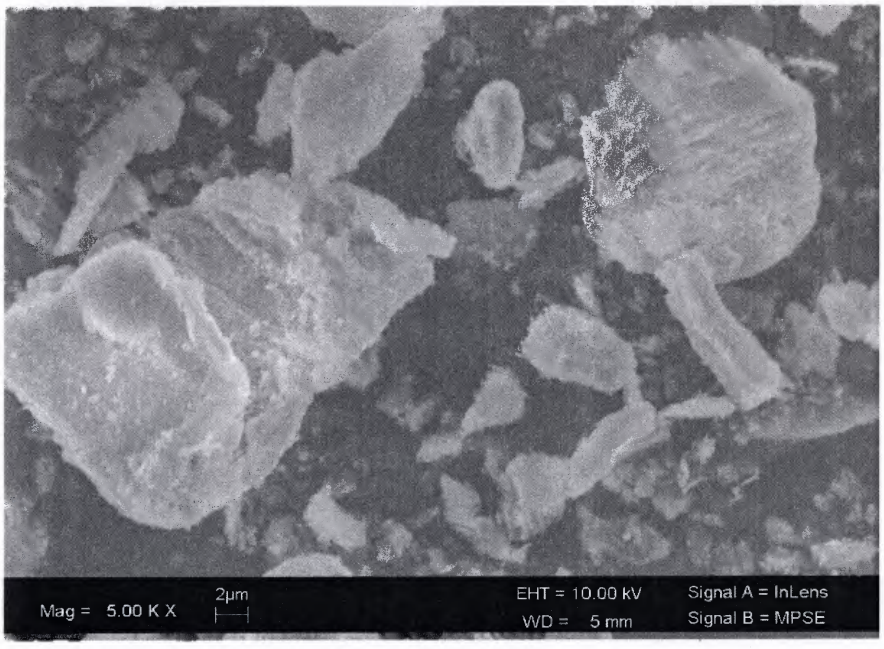

(b)

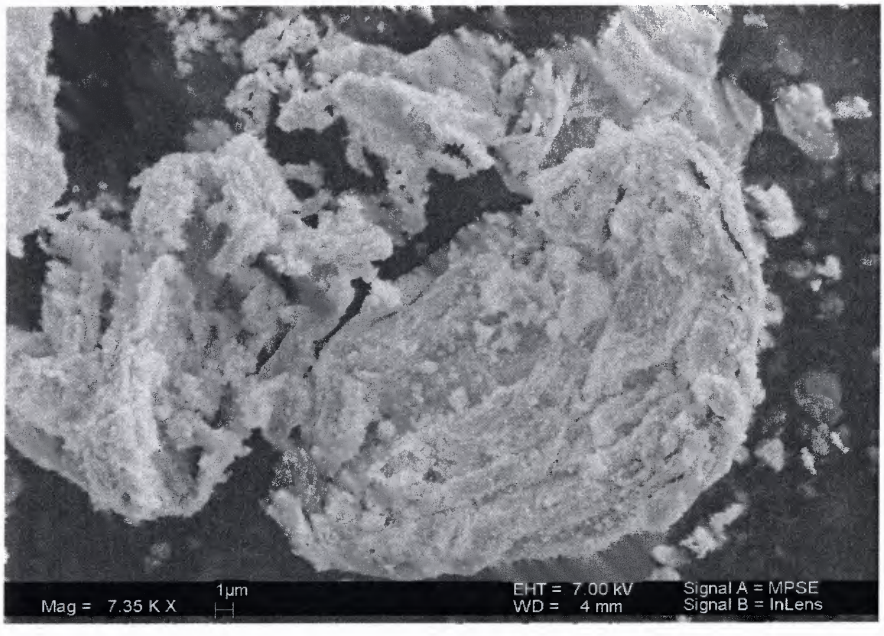

(c)

Figure 4.6 (a), (b) and (c) SEM images of as used MMT. (Continued)

Even though the cryofractured image of PSWNT – 5 (polymer/5 wt% SWNT), Figure 4.7 does not reveal much information, the tensile fractured images of PSWNT - 5, Figure 4.8 (a), (b) and (c) show interesting pictures of agglomerates of well distributed

carbonaceous materials that could SWNT. Images of SWNT with very high aspect ratio embedded in carbonaceous material are shown in Figure 4.9 (a), (b) and (c), representing selected areas of the as received samples.

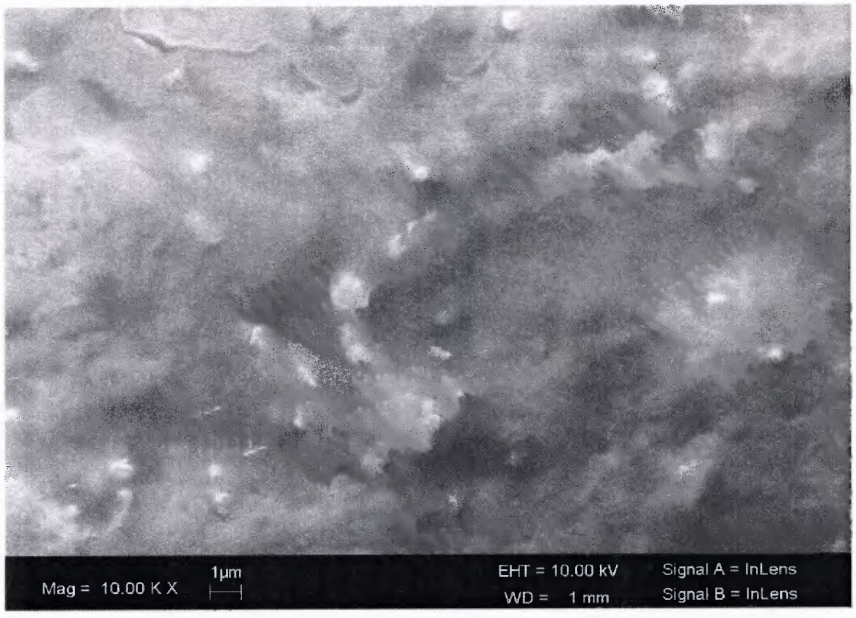

Figure 4.7 SEM image of cryofractured crossection of PSWNT – 5.

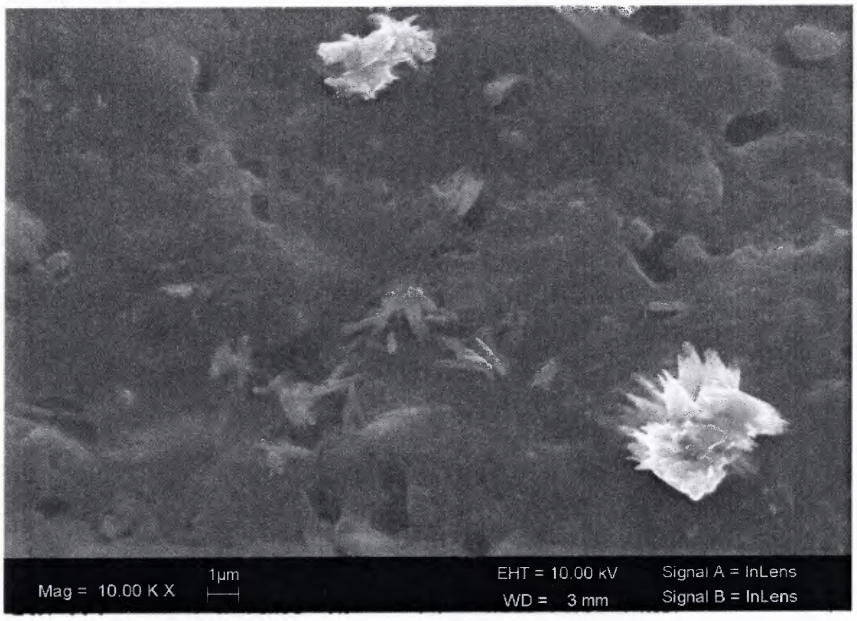

(a)

Figure 4.8 (a), (b) and (c) SEM images of tensile fractured crossection of PSWNT – 5.

(b)

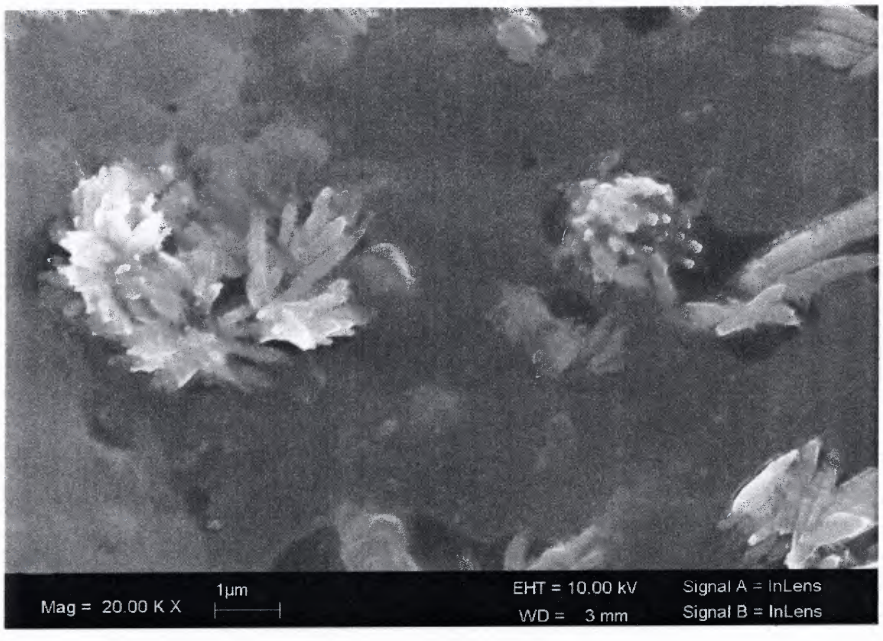

(c)

Figure 4.8 (a), (b) and (c) SEM images of tensile fractured crossection of PSWNT – 5. (Continued)

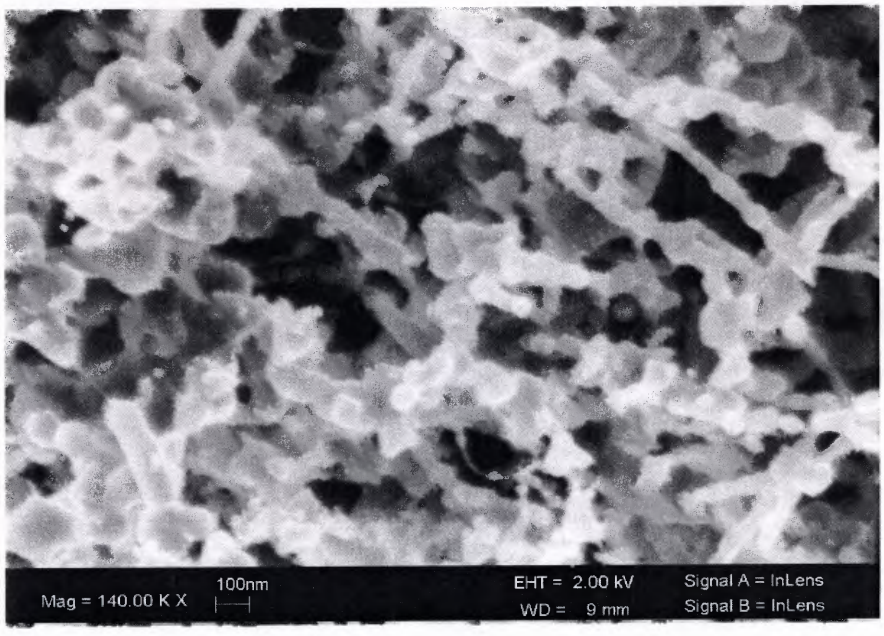

(a)

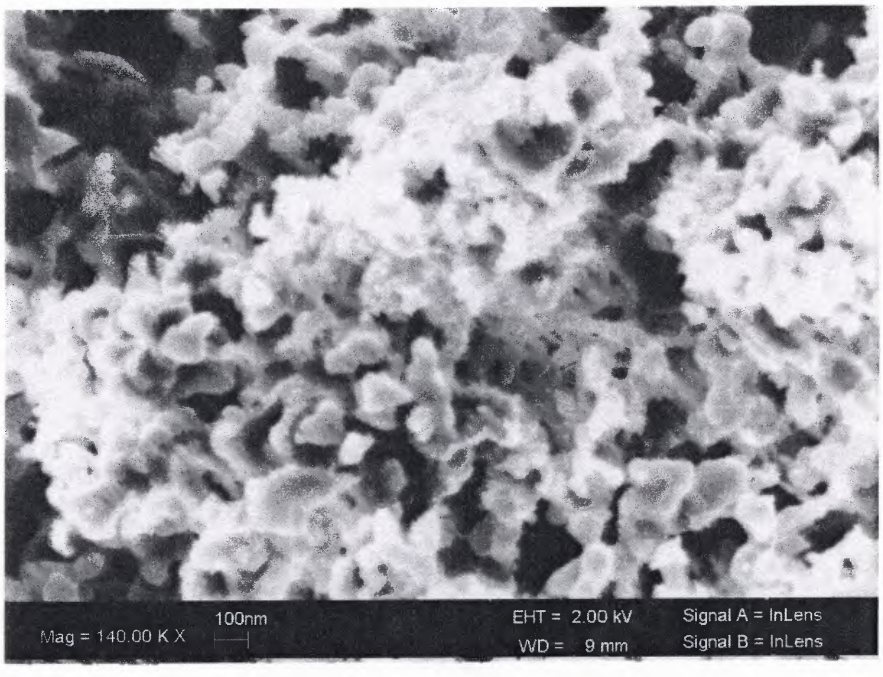

(b)

Figure 4.9 (a), (b) and (c) SEM images of as used SWNT.

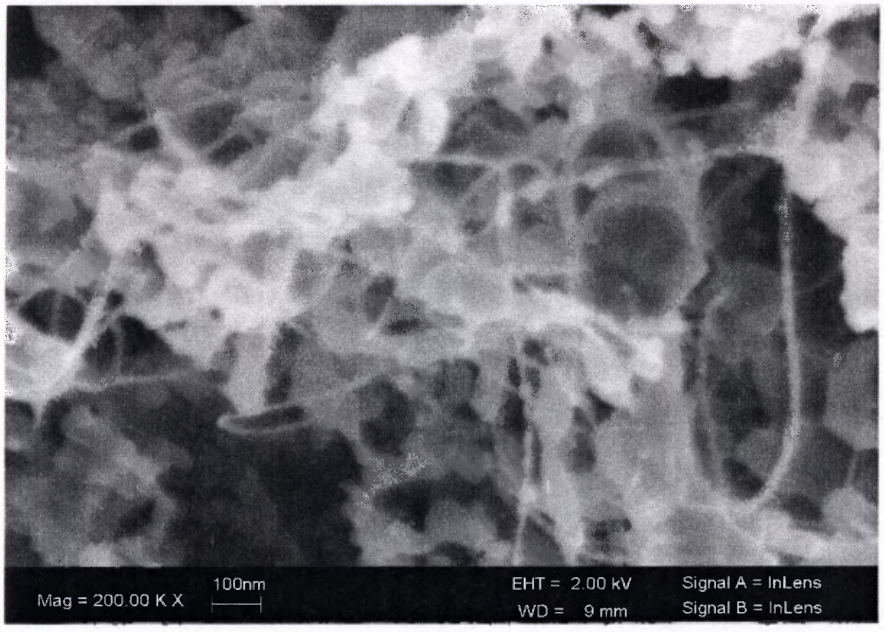

(c)

Figure 4.9 (a), (b) and (c) SEM images of as used SWNT. (Continued)

Figure 4.10 (a) and (b) show images of the sample identified as fullerene (FUL) consisting of a variety of irregular and platey nanoparticles of low aspect ratio. Cross section images of PFUL – 5 (polymer/5 wt% fullerene) are not presented since no distinct features could be seen.

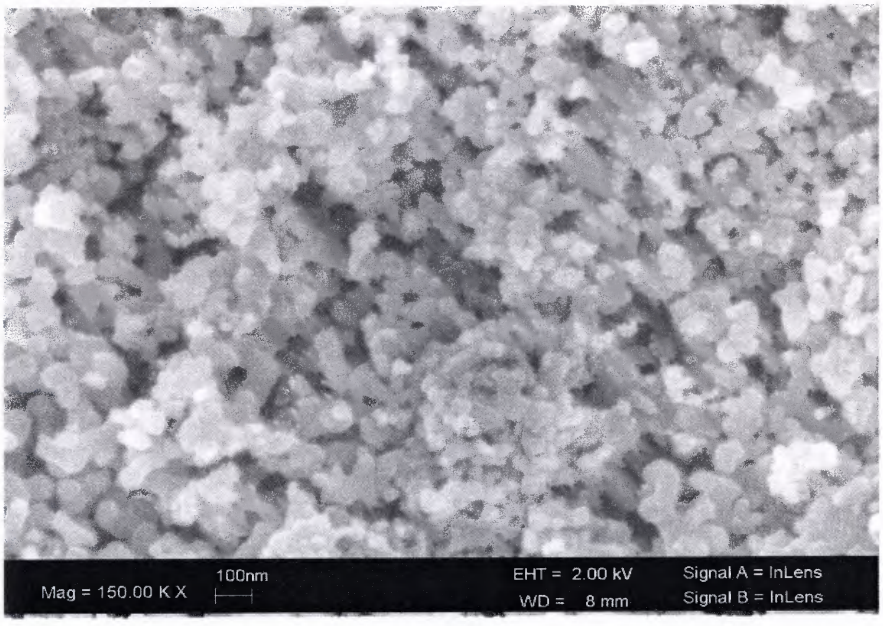

(a)

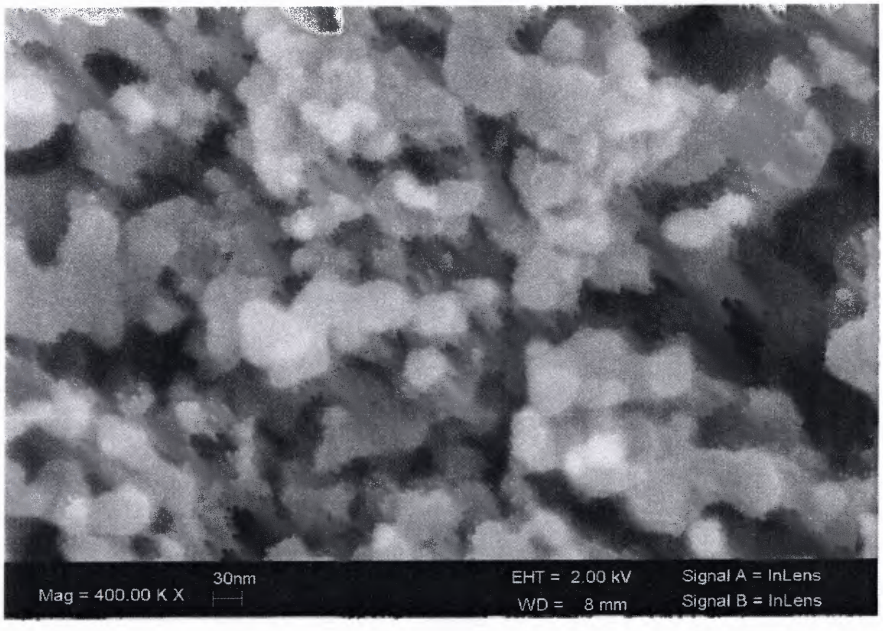

(b)

Figure 4.10 (a) and (b) SEM images of as used FUL.

4.1 Wide Angle X-Ray Diffraction Analysis of Fillers and Composites

Scanning electron microscopy images alone are not sufficient to characterize the nanocomposites. Hence, WAXD was used to probe the composite structure due to its easiness and availability. In WAXD, by monitoring the position, shape and intensity of the basal reflections from the distributed nanofillers, specific features of the nanocomposite structure may be identified.

The WAXD patterns of the PACR, as used HT and PHT – 5 are presented in Figure 4.11. This figure shows a strong peak at $2\Theta = 11.45^{\circ}$ for HT, which is due to the gap in the interlayer platelets of the hydrotalcite clay and it corresponds to a d_{001} spacing of 7.77A°. However, in the PHT – 5 composite, a new peak appears at a lower angle of $2\Theta = 3.65^{\circ}$, which corresponds to an interlayer d_{001} spacing of 24.18A°. This may be due to partial intercalation of the HT by PACR. In addition to the increase in the d_{001} spacing of hydrotalcite, there is also a slight loss in intensity of the basal reflection of HT presumably due to partial exfoliation of HT by PACR. Hence, the PHT – 5 composite corresponds to a hybrid structure consisting of partially exfoliated and intercalated HT.

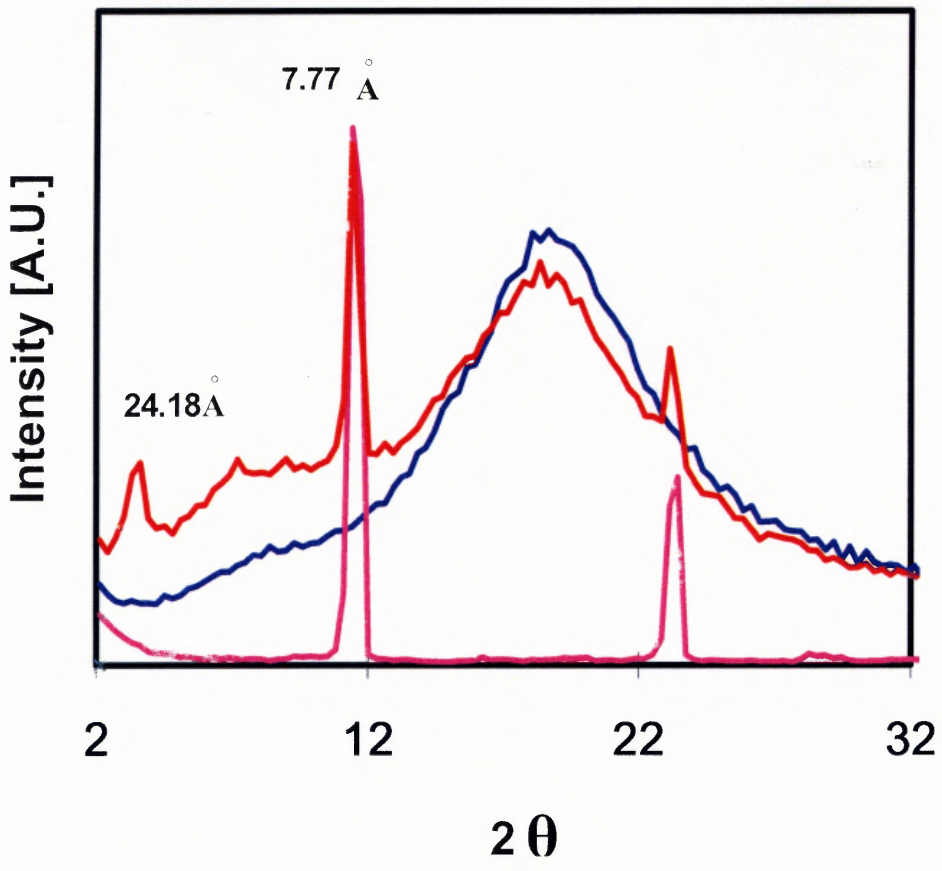

Figure 4.11 WAXRD patterns of PACR (——), HT (——) and PHT – 5 (——).

The WAXD patterns of PACR, MMT clay and PMMT – 5 are shown in Figure 4.12. This Figure shows a peak at $2\Theta = 8.41^{\circ}$ for MMT, which corresponds to a d_{001} spacing of ~10.26A°. This peak is shifted to a lower angle of $2\Theta = 5.15^{\circ}$ (d_{001} = 17.16A°) in the PMMT – 5 composite. This increase in the interlayer spacing indicates that MMT is intercalated by PACR.

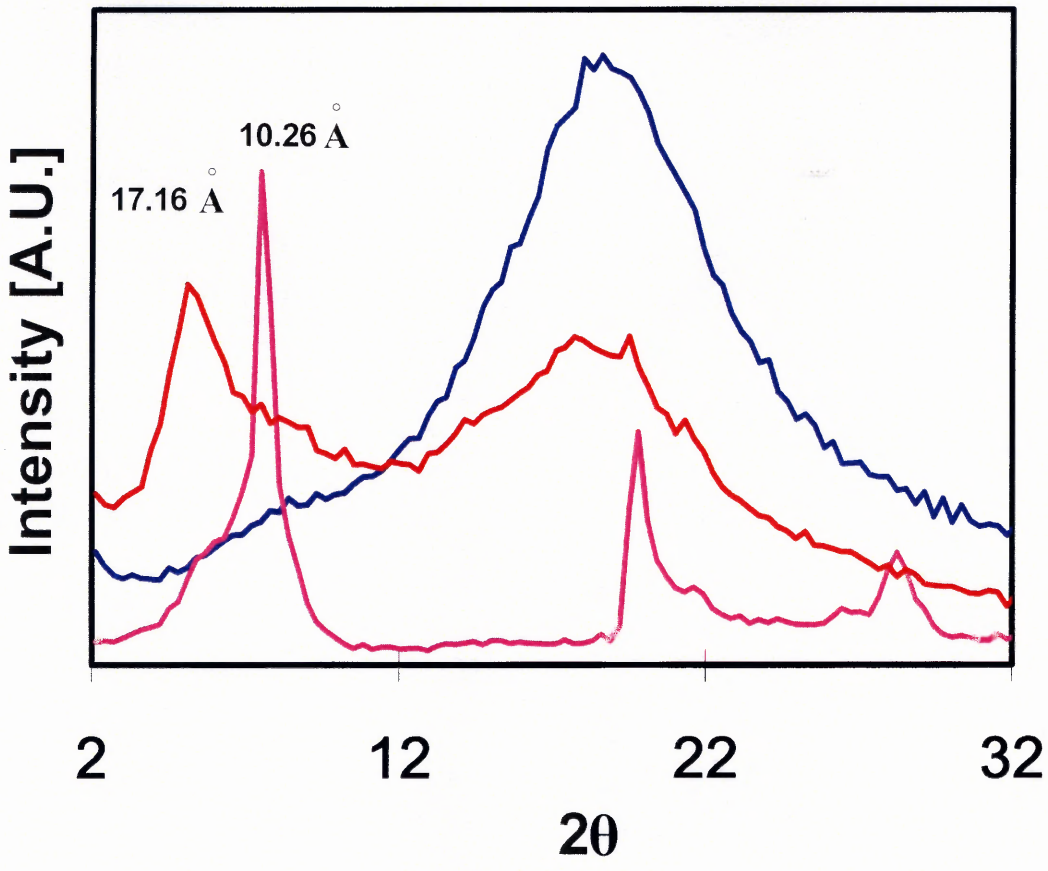

Figure 4.12 WAXRD patterns of PACR (—), MMT (—) and PMMT – 5 (—).

Figure 4.13 and Figure 4.14 represent the WAXD patterns obtained for SWNT (PSWNT – 5) and fullerene (PFUL – 5) based composites containing 5 wt% loading of fillers, respectively. In contrast to the composites filled with nanoplatelets, no appreciable changes were observed in the XRD patterns and further studies using TEM would be required to draw any conclusion since TEM allows for qualitative understanding of the internal structure, spatial distribution of the various phases, and views of the structure through direct visualization.

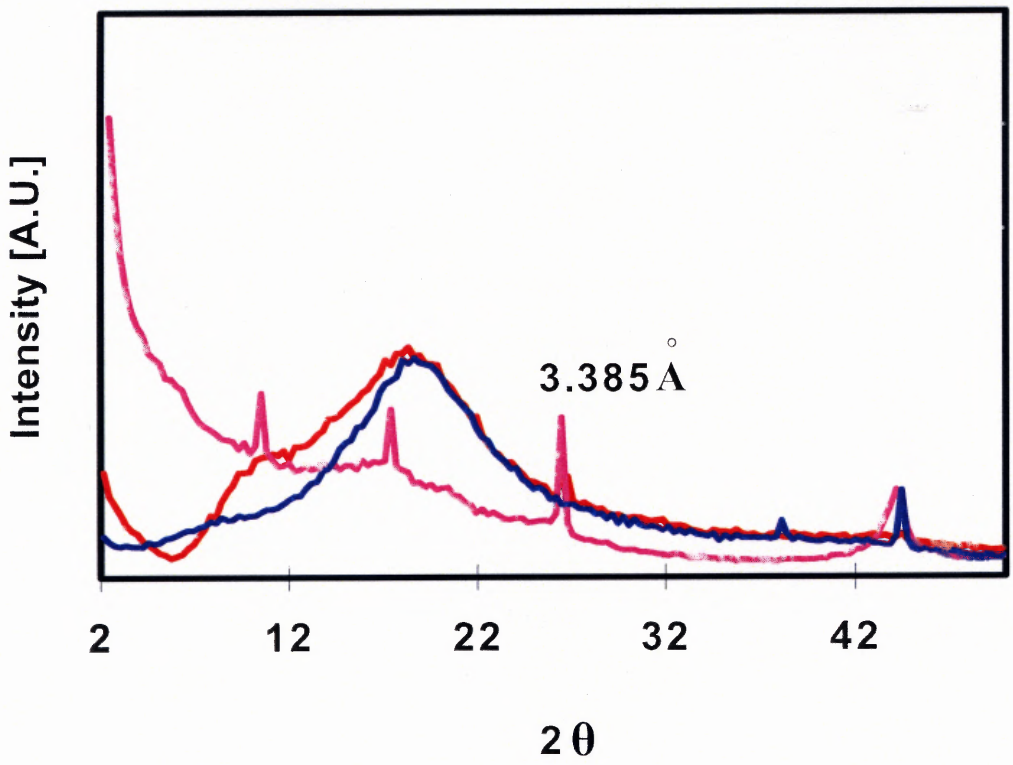

Figure 4.13 WAXRD patterns of PACR (—), SWNT (—) and PSWNT – 5 (—).

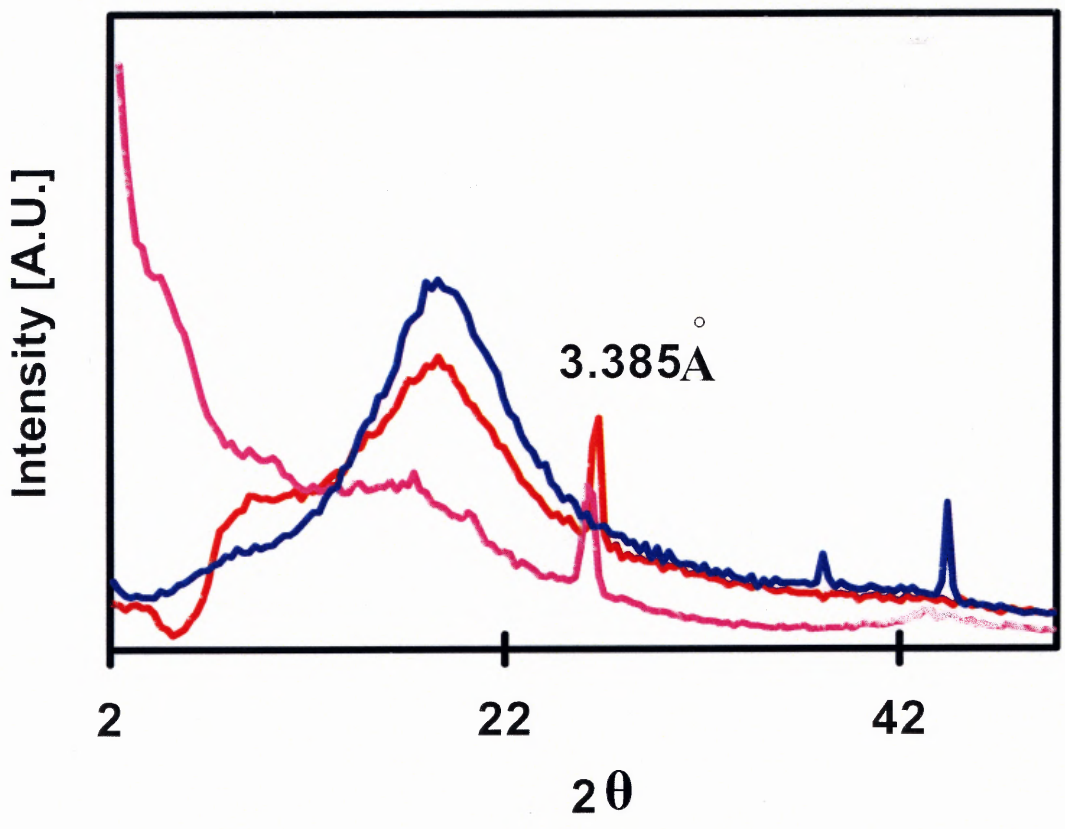

Figure 4.14 WAXRD of PACR (—), FUL (—) and PFUL – 5 (—).

4.3 Mechanical Properties

As mentioned earlier, modification of mechanical properties is one of the most compelling reasons for addition of fillers to polymers. In this section, the results obtained for tensile strength and elongation at break, 2% secant modulus and dynamic mechanical analysis results for stresses applied only in tension are reported for all the composites studied.

Multiple readings per composite were taken to estimate the precision of the reported tensile property data. Statistical analysis appeared to be necessary due to the

variations in results. Average values (AVR) were calculated from the multiple readings (n) and the standard deviation (STDEV) was calculated as shown in Equation 4.1. Values of coefficient of variation (CV) were calculated using Equation 4.2, this was necessary in order to measure the reliability of the results.

$$STDEV = [\{n\sum x^2 - (\sum x)^2\} / n(n-1)]^{1/2} \quad (4.1)$$

$$CV = STDEV / AVR * 100 \quad (4.2)$$

4.3.1 Tensile Properties

Table 4.1 contains tensile property data of PACR and its composites made with different fillers at 5 and 10 wt% filler concentration. This Table provides information on the engineering tensile strength and elongation at break, and 2% secant modulus results of composites in the draw down direction. Figures 4.15, 4.16 and 4.17 show relative changes of tensile strength at break, elongation at break and 2% secant modulus for all composites, versus the unfilled matrix. As expected, the tensile properties depend on the inherent properties of the filler, filler shape and size, extent of interaction at the phase boundaries, and the dispersion and orientation of the fillers in the polymer matrix. It should be noted that caution is required in the interpretation of the results and the identification of trends given the relatively high CV's and small number of specimens tested for some compositions.

Table 4.1 Mechanical Properties of PACR and its Nanocomposites in the Draw Down Direction

Sample	Tensile Strength at Break (MPa)	Elongation at Break (%)	2% Secant Modulus (MPa)
PACR	9.41 ± 0.78 (n = 5; CV = 8.3%)	466 ± 23 (n = 5; CV = 4.9%)	44.3 ± 13 (n = 4; CV = 29.3%)
PHT – 5	5.37 ± 0.78 (n = 4; CV = 14.5%)	430 ± 46 (n = 4; CV = 10.7%)	74.12 ± 4 (n = 2; CV=5.4%)
PMMT – 5	8.61 ± 0.6 (n = 5; CV = 6.9%)	462 ± 19 (n = 5; CV = 4.1%)	56.9 ± 24 (n = 4; CV=42%)
PSWNT – 5	10.09 ± 0.6 (n = 8; CV = 5.5%)	341 ± 52 (n = 8; CV = 15.2%)	75.6 ± 18 (n = 5; CV=23.8%)
PFUL – 5	7.21 ± 0.6 (n = 3; CV = 8.3%)	204 ± 39 (n = 3; CV = 19%)	no measurement
PMMT – 10	no measurement	no measurement	242 ± 117 (n = 3; CV=48%)
PSWNT – 10	no measurement	no measurement	98.4 ± 18 (n = 3; CV=18.3%)

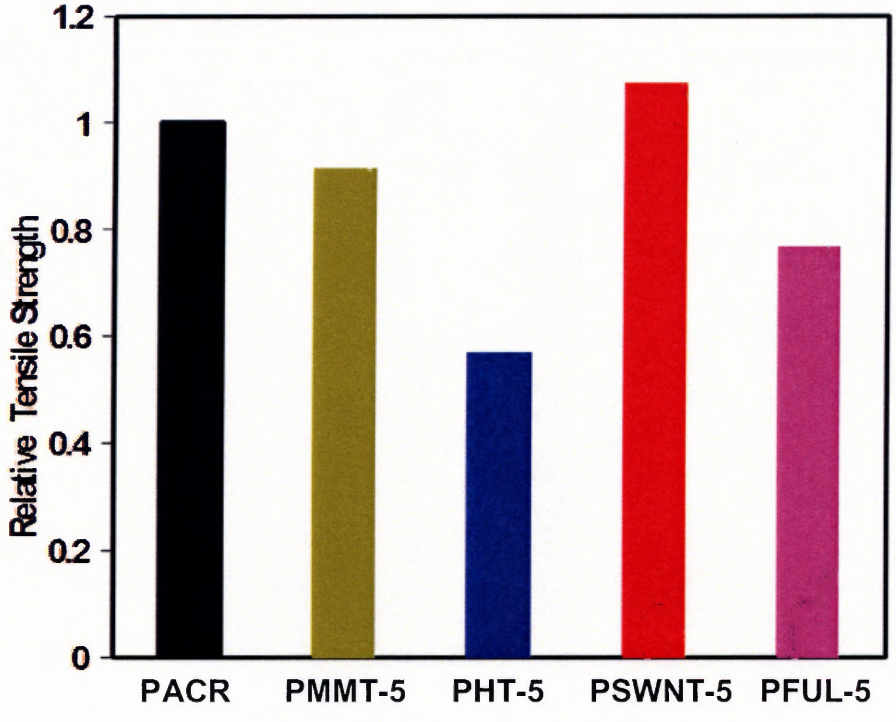

Figure 4.15 Relative tensile strength at break of PACR and its composites.

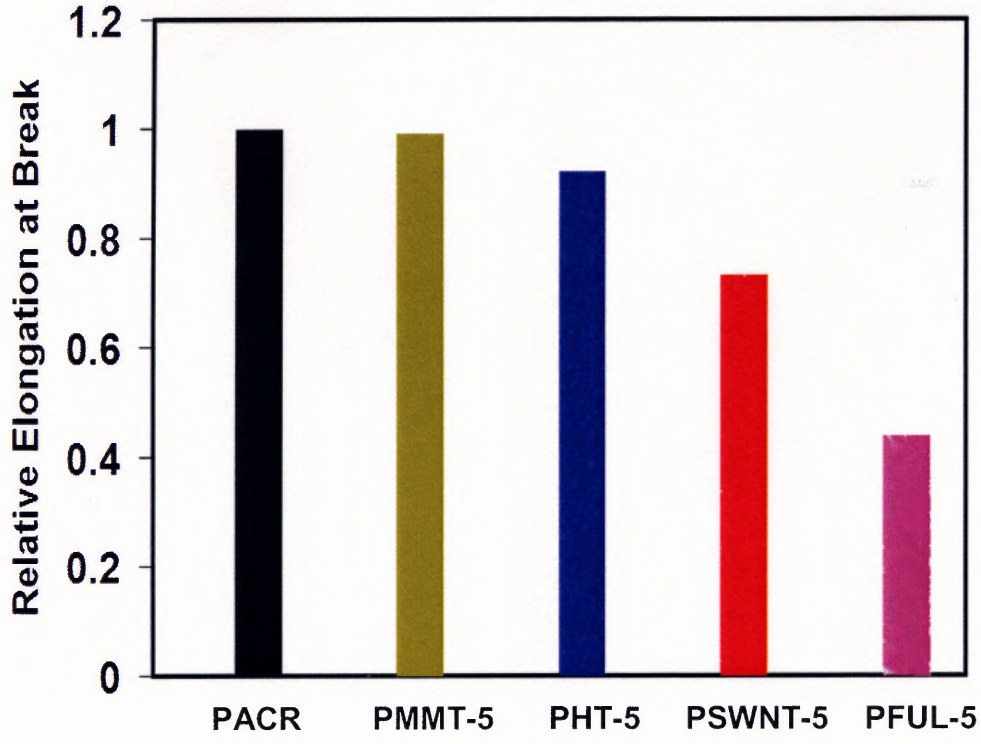

Figure 4.16 Relative elongation at break of PACR and its composites.

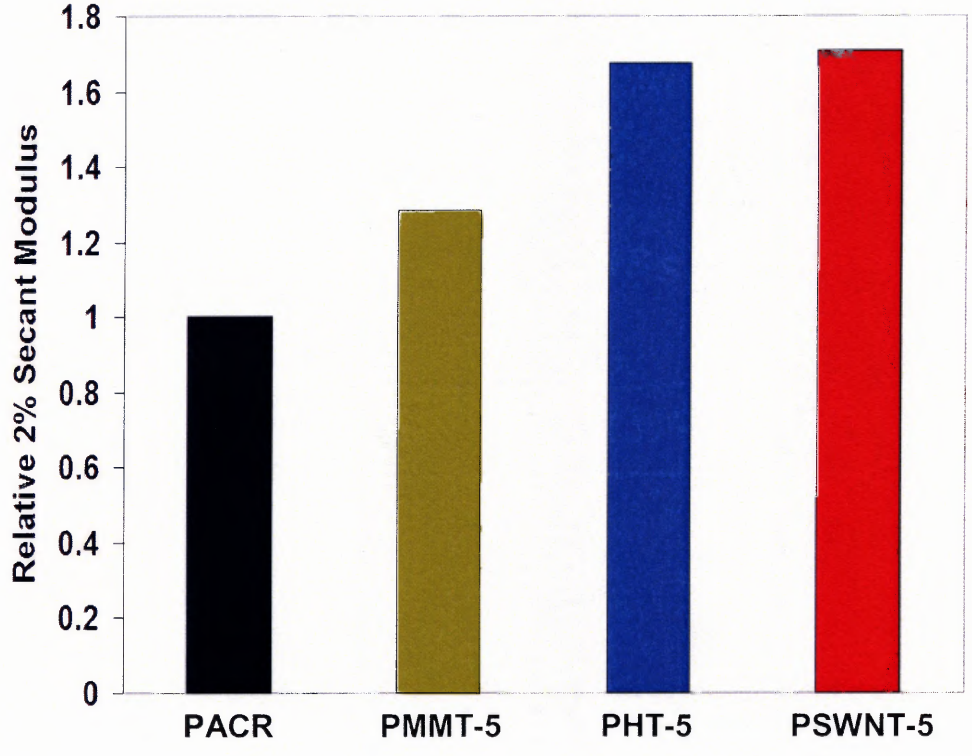

Figure 4.17 Relative 2% secant modulus of PACR and its composites.

Figures 4.15 and 4.16 show that the presence of 5 wt% HT in PACR results in lower tensile strength and elongation at break, respectively. However, Figure 4.17 shows that there is an increase of over 70% in the 2% secant modulus of PACR with 5 wt% HT. This appreciable improvement in the elastic modulus of the PHT – 5 composite may be the result of the partial exfoliation of the HT filler in the PACR since the improvement of modulus directly depends upon the aspect ratio of fillers. Exfoliation results in increased aspect ratio of fillers, which, in turn results in increased interfacial interaction between HT and the PACR.

Intercalated composites obtained with the addition of 5 wt% MMT to the acrylic polymer show a relative increase in the 2% secant modulus, as can be seen in Figure 4.17. However, the tensile strength at break decreases somewhat and there is also a marginal decrease in the elongation at break, as shown in Figures 4.15 and 4.16, respectively. The different effects of HT and MMT on the mechanical properties of the polymer may be attributed to difference in the inherent modulus of the filler, extent of interfacial interaction, aspect ratio and orientation.

Figures 4.15, 4.16 and 4.17 show that while the elongation at break was slightly reduced by the presence of 5 wt% SWNT filler, the 2% secant modulus increased by nearly 70% and a marginal improvement in tensile strength at break was observed. This improvement in mechanical properties may be due to more efficient load transfer between the matrix and the SWNT, as well as the alignment of the SWNT in the polymer matrix. However, it is reasonable to believe that the presence of the carbonaceous material impurities along with the SWNT, and the degradation of carbon nanotubes during processing (reduction in length during sonication) might have contributed to the

low properties of the composite. To elucidate on these issues, the dispersion state of SWNT in the polymer was investigated by SEM and XRD. However, very little or no information could be obtained from these two techniques and transmission electron microscopy would be necessary to study further.

The presence of 5 wt% fullerenes in the acrylic polymer resulted in over 20% reduction in tensile strength at break and over 50% decrease in elongation at break, as shown in Figures 4.15 and 4.16, respectively. The presence of fullerenes makes the acrylic polymer less ductile. One of the reasons for the deterioration of properties with fullerene may be due to their very low aspect ratio when compared to the other fillers.

Table 4.1 also provides 2% secant modulus results obtained with 10% loading of MMT (PMMT – 10) and carbon nanotubes (PSWNT – 10) in the acrylic polymer. It is evident that the modulus of the polymer increases over 350 % with an increase in 5 wt% loading of MMT to 10 wt% and only a marginal improvement in modulus was obtained with 5 wt% increase in loading to 10 wt%, for the SWNT filler.

The mechanical properties of composites were measured perpendicularly to the draw down direction in order to confirm the trends predicted in the models, provided in Chapter 2. According to the models, highest modulus and strength in composites with fibers is obtained in the longitudinal case, i.e. at an application angle of 0°. Accordingly, the composite strength and modulus would decrease rapidly with increasing orientation angle, i.e. even a few degrees of misalignment can significantly reduce the strength and modulus. As for the flakes or platelets oriented in a plane, isotropic properties are expected to be achieved in the plane.

Table 4.2 Mechanical Properties of PACR and its Nanocomposites Perpendicularly to the Draw Down Direction

Sample	Tensile Strength at Break (MPa)	Elongation at Break (%)	2% Secant Modulus (MPa)
PACR	no measurement	no measurement	no measurement
PHT – 5	8.32 ± 0.6 (n = 4; CV = 7.2%)	499 ± 49 (n = 4; 9.8%)	no measurement
PMMT – 5	8.18 ± 0.45 (n = 4; CV = 5.5%)	435 ± 10 (n = 4; CV = 2.3%)	247.89 ± 99 (n = 5; CV=40%)
PSWNT – 5	8.73 ± 0.7 (n = 4; CV = 8%)	420 ± 36 (n = 4; CV = 8.6%)	41.85 ± 3.7 (n = 3; CV=8.9%)
PFUL – 5	no measurement	no measurement	no measurement
PMMT – 10	no measurement	no measurement	99.69 ± 33 (n = 5; CV=33%)
PSWNT – 10	no measurement	no measurement	50 ± 14.7 (n = 5; CV=29.4%)

In this context, Table 4.2 provides information on the tensile strength and elongation at break, and 2% secant modulus of composites with different fillers, perpendicular to the draw down direction. These results show deviations from those expected for flakes and platelets; this may be a result of the misalignment of HT and MMT platelets by different angles, relative to the x-y plane and hence isotropy is not achieved. However, as expected, the values of tensile strength at break and the 2% secant modulus of the PSWNT composite are reduced perpendicularly to the draw down direction due to the presence of fibers. For both 10 wt% PMMT and PSWNT, 2% secant modulus is higher in the draw down direction than in the transverse direction. At this juncture it is important to note that, in the above argument, it is assumed that the properties of the acrylic polymer are isotropic.

4.3.2 Dynamic Mechanical Analysis

DMA was used to measure the response of the different composites to an oscillatory deformation as a function of temperature. DMA has been used to study temperature dependence of the storage modulus of PACR and its composites with 10 wt% loading of MMT and SWNT. Variations in tan δ behavior as a function of temperature between the composites are also reported.

Figure 4.18 shows that the storage moduli of PACR, PMMT – 10 and PSWNT – 10 rapidly decreases in the temperature range of -25° to about 40°C, an indication of a possible glass transition temperature. The storage modulus of PACR is increased by the stiffening effect of the fillers, which is particularly significant with MMT clays at higher temperatures, followed by that with SWNT. In the entire temperature range from -40°C to 150°C, the storage modulus of PSWNT – 10 is higher than that of PMMT – 10 in the temperature range from -4°C to 35°C. The modulus of both the composites is more or less the same at 0°C whereas at 150°C PMMT – 10 shows a 7-fold increase and PSWNT – 10 shows a 3-fold increase versus the unfilled PACR.

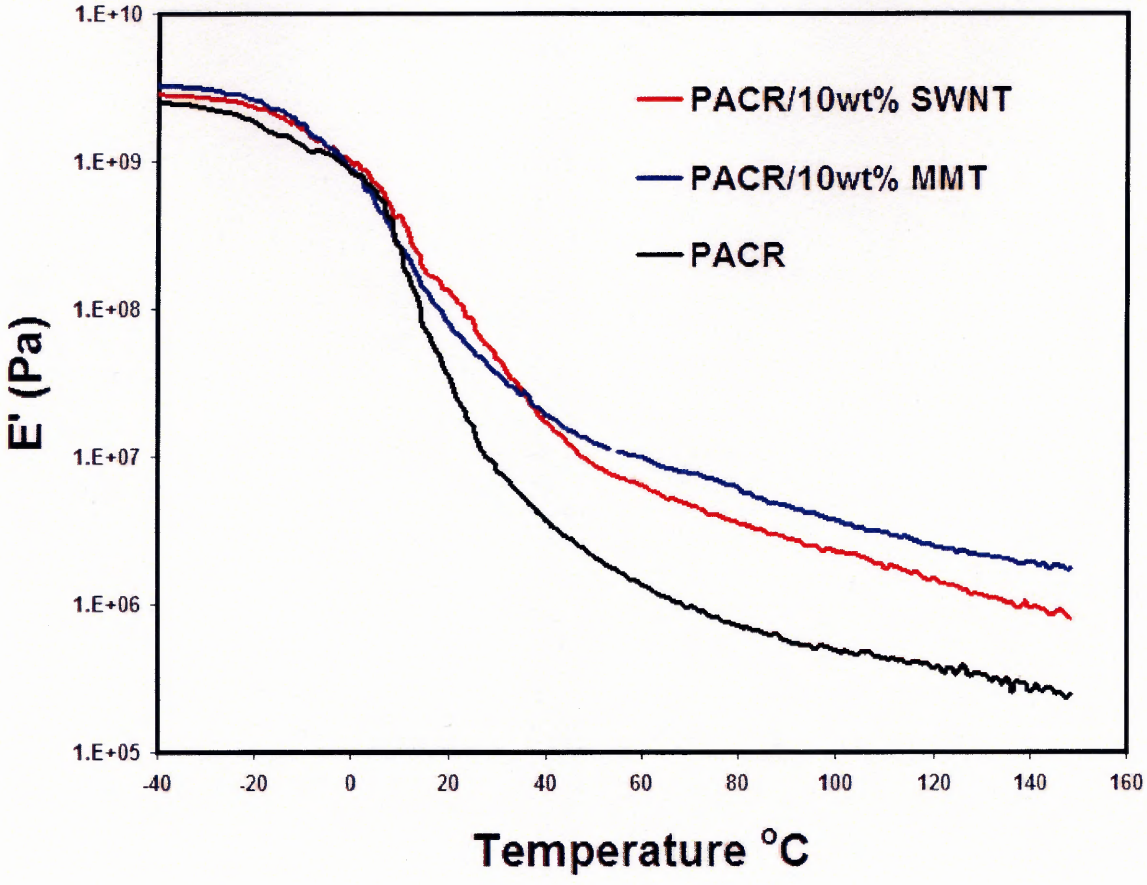

Figure 4.18 Dynamic mechanical spectra of storage modulus for PACR (——), PMMT – 10 (——) and PSWNT – 10 (——).

Figure 4.19 shows variations in the tan δ as a function of temperature for PACR, PMMT – 10 and PSWNT – 10. The Figure shows that PACR has a glass transition temperature at around 20°C. The Figure also shows that the presence of 10 wt% MMT in the acrylic polymer shows some broadening of the peak, and moves the peak to a slightly higher temperature. However, the presence of 10 wt% SWNT only slightly increases the T_g of the acrylic polymer.

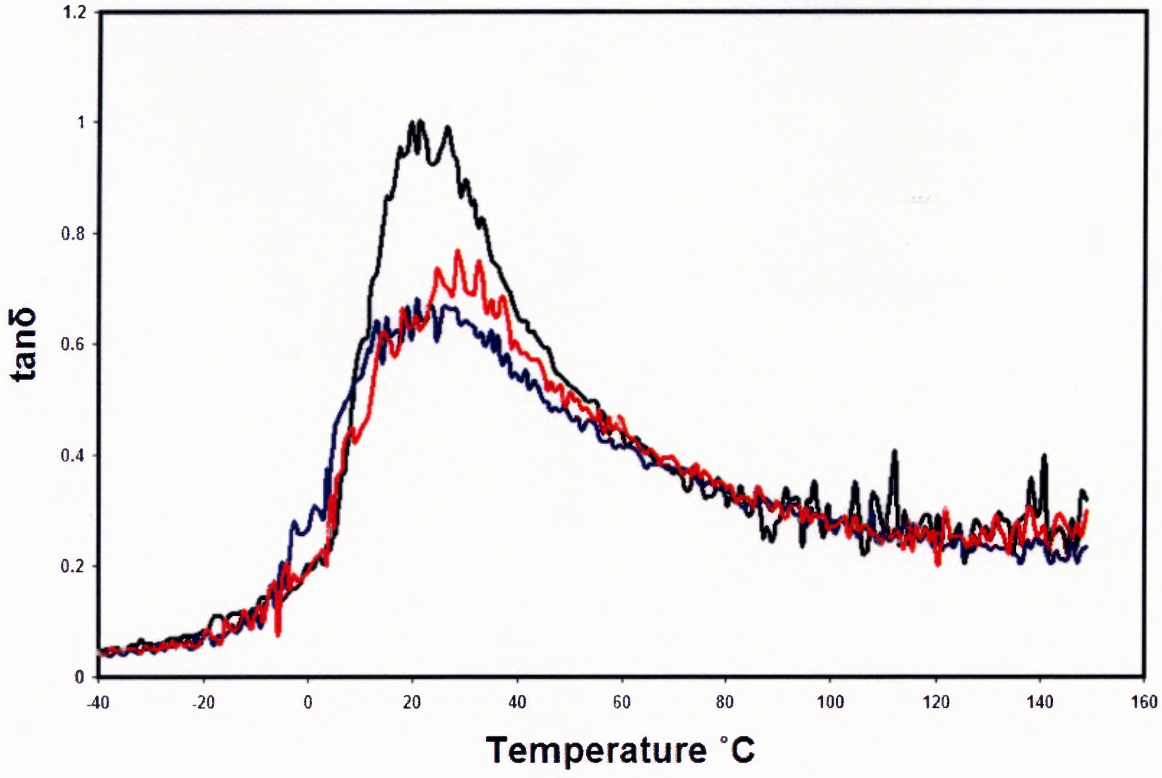

Figure 4.19 Dynamic mechanical spectra of tanδ for PACR (——), PMMT – 10 (——) and PSWNT – 10 (——).

4.4 Thermal Analysis of Fillers and Composites

4.4.1 Differential Scanning Calorimetry Analysis

The DSC technique provides quantitative and qualitative information about the physical and chemical changes that generate or absorb heat as well as changes in heat capacity using minimal amounts of sample. The DSC thermograms for the polymer and all its composites can be found in Appendix B. All specimens were scanned at heating and cooling rates of 15°C/min from -60°C to 200°C in a nitrogen atmosphere in order to take measurements of glass transition temperature and/or melting temperature. However, our experiments did not indicate any melting characteristics in the temperature range of -60° to 200°C as can be seen in the thermograms. DSC heating scans up to 200°C indicated

that a transition temperature corresponding to T_g occurred at about 20°C, similar to the location of tanδ peak, although abrupt changes in heat flow versus temperature curves could not be easily detected. Similar curves were obtained for composites with 5 wt% loading of fillers. Table 4.3 summarizes the glass transition temperatures of PACR and its composites from the plots in Appendix B, to the best of our understanding of the software. The table shows that the presence of 5 wt% HT, MMT and SWNT appears to reduce the glass transition temperature of the polymer. The Table also shows that the presence of 5 wt% FUL appears to increase the T_g of PACR by about 2°C. These results should be viewed with caution given the presence of residual volatiles in a closed DSC pan that could affect the readings.

Table 4.3 Apparent DSC Glass Transition Temperature of PACR and its Nanocomposites

Sample	T_g (°C)
PACR	20.28
PHT – 5	10.34
PMMT – 5	8.59
PSWNT – 5	11.09
PFUL – 5	23.07

4.4.2 Thermogravimetric Analysis

The thermal stability of polymeric materials is usually studied by thermogravimetric analysis (TGA). The weight loss due to the formation of volatile products after degradation at high temperature is monitored as a function of temperature. A non oxidative degradation test was done on the polymer and its composites used in this study. The dried commercial acrylic polymer would contain the 29% of solids originally present in the liquid paint and in addition it will also contain some of the less volatile matter

which did not escape during the drying cycle of 50°C under vacuum for 24 hours. The polymer shows a progressive degradation starting at about 120°C to be completed at 500°C, as seen in Figures 4.20 to 4.25.

In general, the incorporation of platelets into the polymer matrix has been found to enhance its thermal stability by acting as a superior insulator and mass transport barrier to the volatile products generated during decomposition (Ray and Okamoto 2003). However, there have been contradicting results reported in the literature as for example the one obtained for poly(ε – caprolactone) / hydrotalcite nanocomposite by Sorrentino et al. (2005) where no thermal stability improvement was observed.

Figure 4.20 and Figure 4.21 show the results of the TGA thermograms for the unfilled polymer (PACR) and the composites containing 5 wt% HT and MMT, respectively. Form these figures we see that the thermal stability of the composites are not improved in the presence of either filler. This is particularly interesting in the case of MMT where the nonintercalated mineral shows a significant thermal stability up to 500°C. Small differences between PHT – 5 and PMMT – 5 as shown in Figure 4.22 appear to manifest themselves after about 300°C with trends reversed after 430°C. Up to about 320°C, both composites are less stable than the matrix.

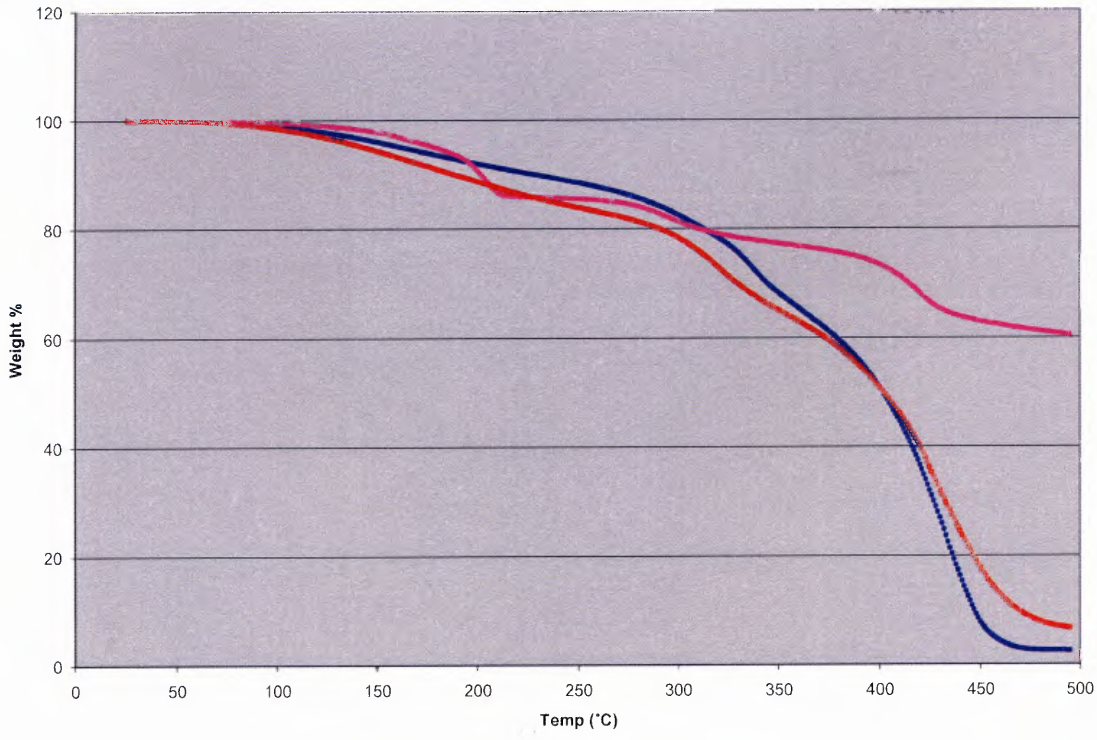

Figure 4.20 TGA thermograms of PACR (—), HT (—) and PHT – 5 (—).

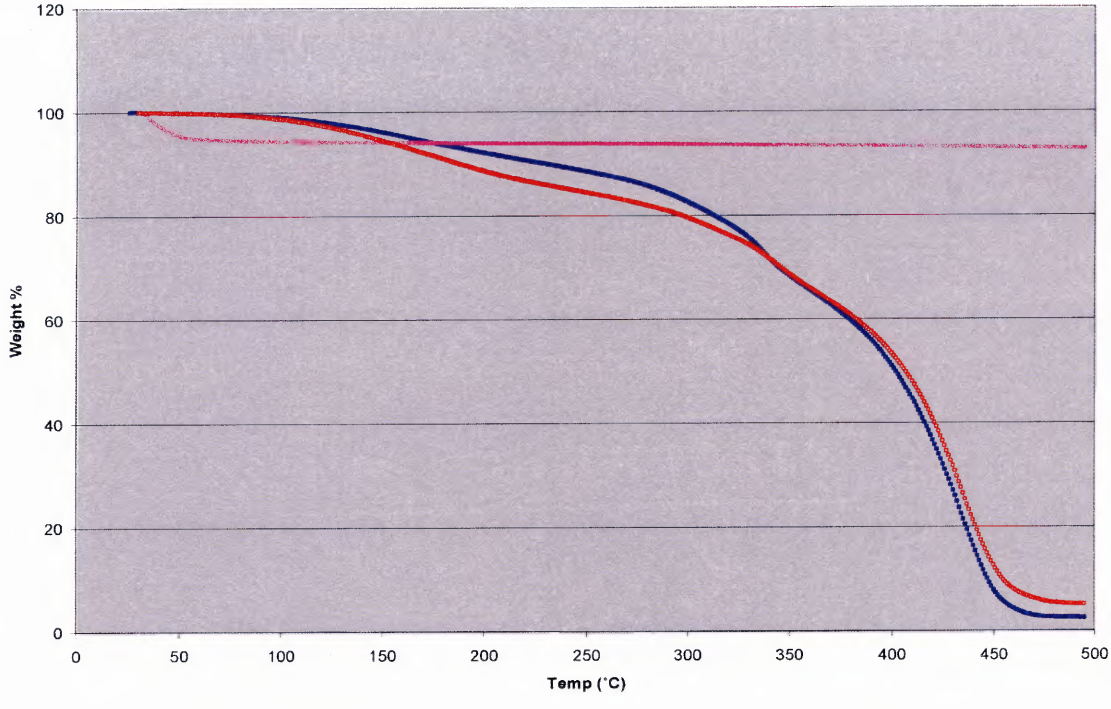

Figure 4.21 TGA thermograms of PACR (—), MMT (—) and PMMT – 5 (—).

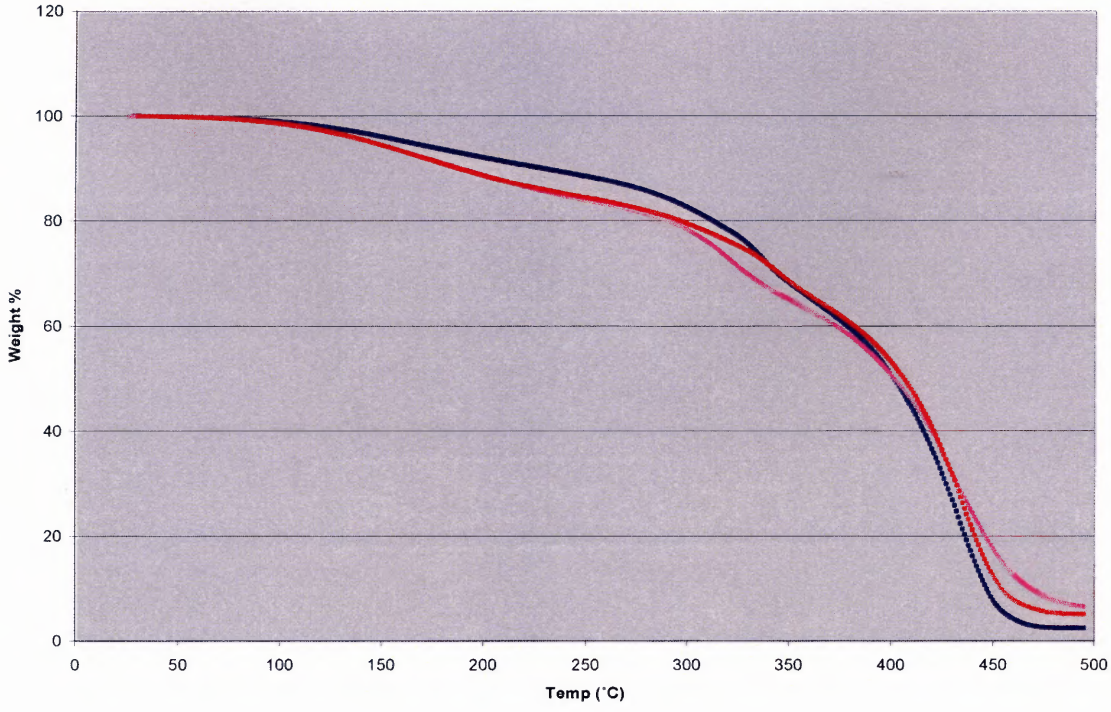

Figure 4.22 TGA thermograms of PACR (—), PHT – 5 (—) and PMMT – 5 (—).

In contrast to the PHT – 5 and PMMT - 5 composites, a notable reduction in the thermal degradation of the acrylic polymer was observed with SWNT and FUL composites at 5 wt% loading as can be seen in Figures 4.23 and 4.24, respectively. At 20% weight loss, the decomposition temperature of the FUL composite PFUL – 5 at 327°C is much higher than that for the SWNT composite PSWNT - 5 at 318°C, which in turn is higher than that of the unfilled acrylic polymer PACR, which is at 313°C. However, at around 50% weight loss, the decomposition temperature of fullerene and SWNT composites become nearly the same and this same trend is observed up to 500°C, as shown in Figure 4.25. Note in Figures 4.23 and 4.24 the high thermal stability of both SWNT and FUL fillers.

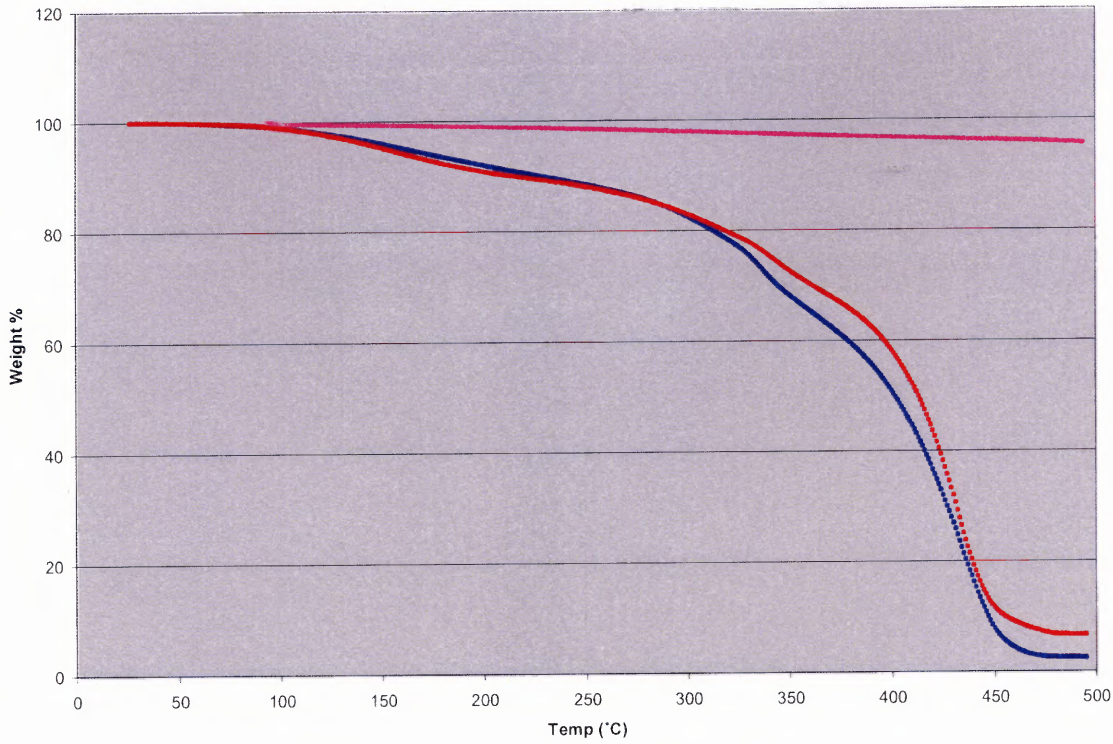

Figure 4.23 TGA thermograms of PACR (—), SWNT (—) and PSWNT – 5 (—).

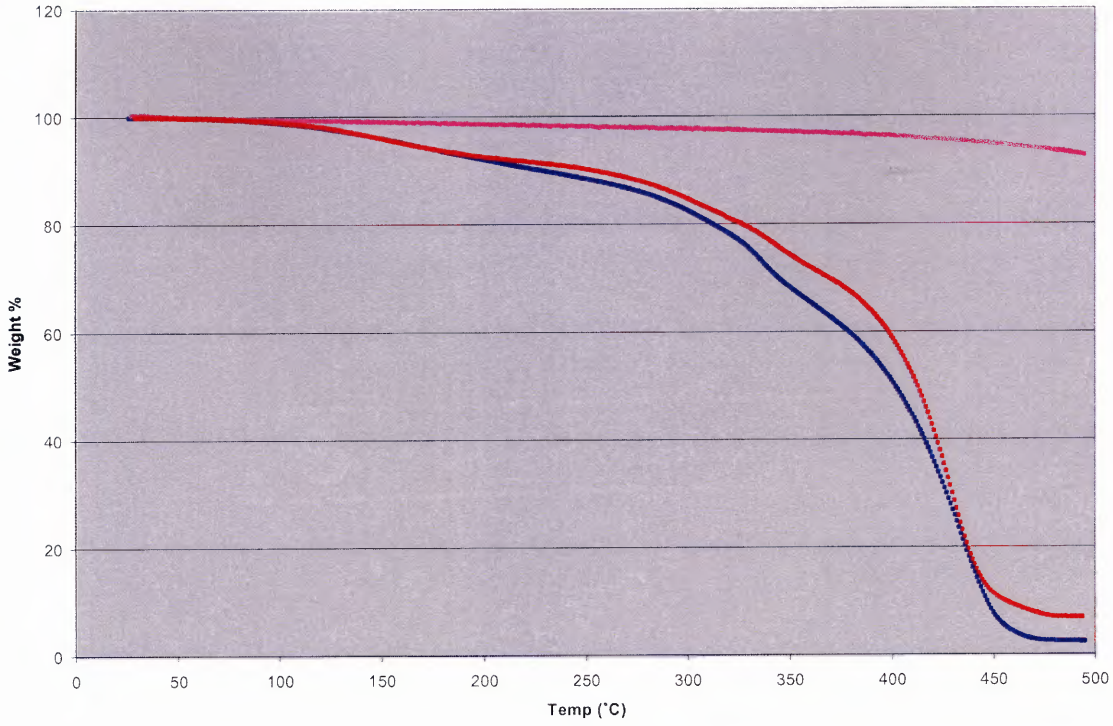

Figure 4.24 TGA thermograms of PACR (—), FUL (—) and PFUL – 5 (—).

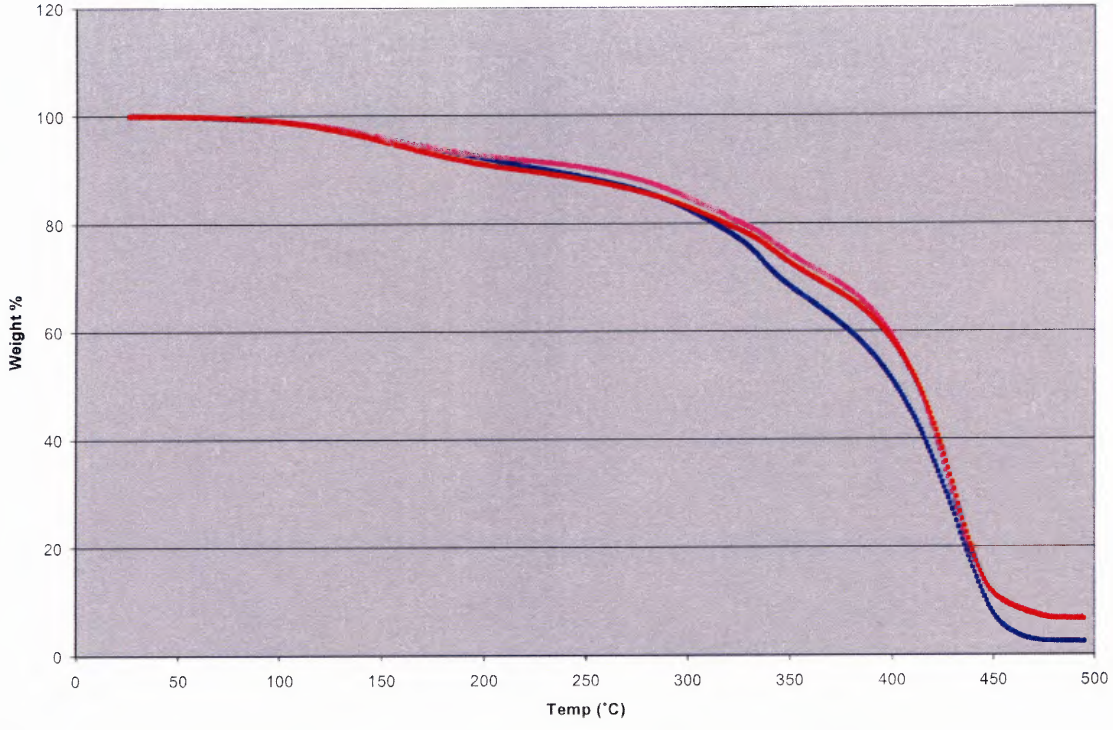

Figure 4.25 TGA thermograms of PACR (—), PFUL – 5 (—) and PSWNT – 5 (—).

4.5 Barrier Properties

The barrier properties of the composites with 5 wt% loading of different fillers and that of the film without the fillers were tested using the ASTM E-96 standard, at room temperature. Specifically, the water method was used for testing the property. With such comparison one would expect that the presence of the filler, spherical, platelet, fiber, etc. would introduce a tortuous path for the diffusing permeant.

Figures C.1 to C.9 in Appendix C depict the plots of weight versus time for the composites obtained from the water vapor permeability testing, whereas Table 4.4 summarizes the results obtained from those Figures using Equation 3.2.

Table 4.4 WVTR of PACR and its Nanocomposites with 5 wt% loading

Sample	Thickness (mm)	WVTR ($g/hr.m^2$)	Average WVTR ($g/hr.m^2$)
PACR	0.254	0.00183	0.00166
PACR	0.254	0.00149	
PHT - 5	0.4318	0.00184	0.00165
PHT – 5	0.4445	0.00145	
PMMT - 5	0.3810	0.00147	0.00117
PMMT - 5	0.264	0.00087	
PSWNT - 5	0.2540	0.00114	0.001135
PSWNT - 5	0.3430	0.00113	
PFUL - 5	0.2032	0.00126	0.00126

The data in Table 4.4 should be interpreted with caution since:

(a) A minimum of two specimens were used for each composite with PFUL – 5 tested only once.

(b) Thickness of the specimens varied and was not taken into account to calculate WVTR as suggested by ASTM E-96.

In spite of the variability of the data it can be shown that all fillers and in particular, the hydrophobic SWNT and FUL may reduce water vapor transmission rate.

Table 4.4 shows that the water vapor transmission rate of the composites containing HT is nearly the same as that for the PACR. It is known that the barrier property of the composites greatly depends not only on the polymer structure but also on the structure and properties of the nanofiller. Factors such as aspect ratio, surface area, extent of dispersion and orientation of nanofillers also have a great influence on permeability of the polymer matrix. Further more, the water vapor transport through the polymeric films proceeds through sorption, diffusion and desorption of water vapor. So, on one hand the presence of the low aspect ratio HT platelets ought to increase to some extent the tortuosity of the system, leading to an expected decrease in the value of the diffusion coefficient. On the other hand, with partially exfoliated and intercalated HT layers one can expect that more and more of these specific HT particles may act as preferred sites on which the water vapor molecules are adsorbed and/or immobilized due to their hydrophilic nature. This could result in an increase in weight of the system and hence the WVTR of the PHT – 5 obtained would be nearly the same as that for PACR. However, it is reasonable to assume that these specific HT sites in the matrix have finite capacity for sorption depending on its concentration and texture and when these sites would be occupied there will be a further decrease in WVTR.

Measurement of WVTR of PMMT - 5 composites showed a decrease in WVTR. MMT platelets have a high aspect ratio and this geometry favors the reduction in permeability by forcing diffusing molecules to take a long way around the platelets. A simple tortuous two dimensional model has been developed by Nielsen (Equation 2.8) to

depict the effect of the size of the fillers on the barrier properties of the polymer composites containing platelet particles. Even though, montmorillonite clay is also hydrophilic in nature, increased resistance to permeability may be due to less sorption of water molecules on the clay particles due to greater interactions between the MMT and the PACR; this can be justified by the enhanced 2% secant modulus seen in the results of the mechanical tensile testing (Table 4.1).

The water vapor permeability of polymer films containing SWNT and FUL is lower than that of the polymer film. Furhter more, composites containing SWNT show more resistance than those for FUL. This decrease in WVTR is expected since both fillers are hydrophobic resulting in zero sorption of water molecules and both the fillers are also impermeable to water. Due to the higher aspect ratio of the carbon nanotubes when compared to that of the fullerenes, a more tortuous path for the diffusing permeant molecules would be created and thus decrease the effective cross sectional area available for diffusion.

CHAPTER 5

CONCLUSIONS

The present work was initiated to explore the preparation and characteristics of polymer nanocomposites with a focus on modifying the properties of a commercially available acrylic polymer paint. Incorporated nanofillers included hydrotalcite, sodium montmorillonite, and impure single walled carbon nanotubes and fullerenes with different size, shape and aspect ratio. During the last few decades, significant interest has been developed in the area of such polymer composites because it has become evident that the next technological frontiers will be achieved not by a better understanding and application of a particular material, but rather by understanding and optimizing materials combinations.

Composites were produced by a combination of solution mixing and solvent casting at 5 and 10 wt% loading of fillers, with the aid of sonication. An anionic surfactant was added to facilitate dispersion of nanotubes and fullerenes. Unfilled polymer samples were also prepared for comparison studies. Significant differences were noted following the determination of the mechanical, thermal and barrier properties of the composites. The morphology of the composites was studied using scanning electron microscopy and wide angle X-ray diffraction.

SEM images show that HT and MMT platelets are well distributed in the acrylic polymer with incomplete alignment of the platelets in the plane of draw down. XRD results indicate that while the HT platelets are partially exfoliated and intercalated by the acrylic polymer, MMT clays are only intercalated by the polymer. SEM images of the

nanotube composites show interesting pictures of well distributed carbonaceous materials that could also contain nanotubes. XRD results of nanotube and fullerene composites did not provide any information on degree of dispersion. The SEM images of the fullerene composite showed no distinct features.

On comparison of the mechanical properties of 5 wt% loading of HT and MMT composites with those of the PACR, PMMT – 5 showed only a marginal decrease in tensile strength and elongation at break when compared to PACR, while PHT – 5 showed a greater decrease in tensile strength and elongation at break. However, the 2% secant modulus of PHT – 5 was significantly enhanced due to the partial exfoliation and intercalation of HT by the PACR and a less significant improvement in modulus of PMMT – 5 was observed when compared to that of the PACR, as a result of intercalation of MMT by the PACR.

PACR containing 5 wt% SWNT shows a higher tensile strength and 2% secant modulus with a relative decrease in elongation at break. PACR containing 5 wt% FUL shows a decrease in tensile strength and elongation at break.

PACR containing 10 wt% MMT and SWNT shows an increase in the 2% tensile secant modulus and storage modulus of the polymer. DMA plots of tanδ versus temperature shows that the presence of 10 wt% MMT and SWNT in the PACR shifts the tanδ peak corresponding to the T_g to a slightly higher temperature.

Mechanical properties tested perpendicularly to the draw down direction indicate that the SWNT could be aligned in the composite while the nanoplatelet composites indicate a misalignment of platelets at different angles, relative to the x-y plane.

DSC heating scans up to 200°C indicated that a transition temperature corresponding to T_g occurred at about 20°C, similar to the location of tanδ peak, although abrupt changes in heat flow versus temperature curves could not be easily detected. Similarly, curves for composites with 5 wt% HT, MMT and SWNT suggest lower T_g and composites with 5 wt% FUL suggest a slightly higher T_g. The results should be viewed with caution given the presence of residual volatiles in a closed DSC pan and our understanding of the software used for measuring T_g that could lead to different interpretations. TGA thermograms of the composites show that the presence of 5 wt% nanoplatelets does not increase the thermal stability of the polymer. In contrast to the nanoplatelet composites, a notable reduction in the thermal degradation of the acrylic polymer was observed with SWNT and FUL composites at 5 wt% loading.

Transmision of water vapor through the composites with 5 wt% loading of fillers, shows a decrease in rate when compared to that of PACR. This reduction in transmission of water vapor through the composites varies to different extents depending on the aspect ratio, inherent properties, extent of dispersion and orientation and interfacial interaction of the filler with the polymer.

The above conclusions on the mechanical and barrier properties of composites are drawn from only a few specimens that have been tested. Hence, future work should involve synthesis and testing of a greater number of specimens for each type of composite in order to improve the reliability of the reported data. Dynamic mechanical analysis of the composites with 5 wt% loading of fillers needs to be done in order to compare the tanδ results with that of the T_g obtained from DSC tests.

Even though the presence of single walled nanotubes in the polymer shows an improvement in the mechanical properties of the polymer, further improvements in the properties can be envisaged by the use of purified nanotube samples.

It is important to understand the mechanism of enhancement of major physical and engineering properties prior to further usage of these fillers. For this to be achieved, it is important that comparison with existing models and generation of new models are made for various systems. Certain issues that need to be addressed for modeling include the extent of dispersion, aspect ratio retention and orientation of the fillers. Transmission electron microscopy of the fillers and composites needs to be done in order to provide insight into these issues.

APPENDIX A

ENERGY DISPERSIVE X-RAY PLOTS

In this appendix, EDX elemental analysis plots of the fillers used in making the composites are presented.

Figures A.1, A.2, A.3 and A.4 represent the EDX results for hydrotalcite, sodium montmorillonite, carbon nanotubes and fullerenes in carbon allotropes, respectively. The EDX results provide quantitative information on the constituents of the respective fillers.

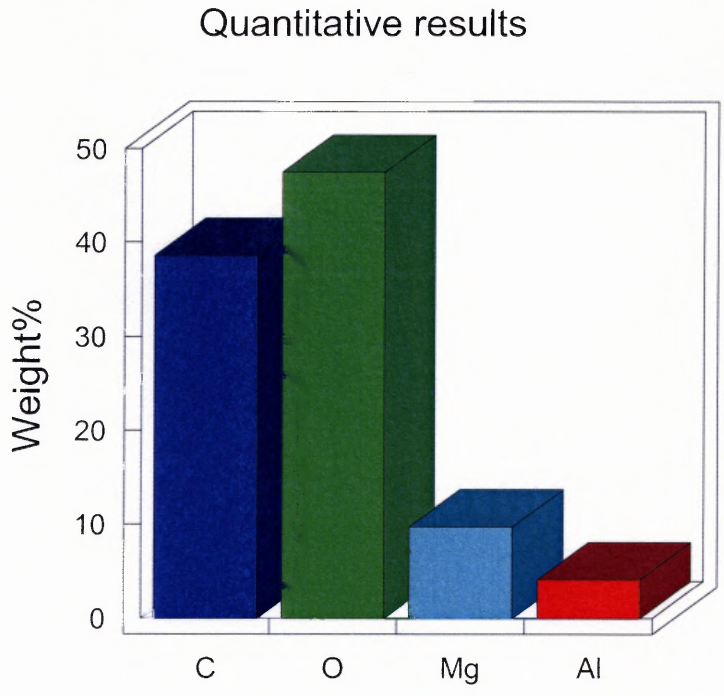

Figure A.1 EDX result of hydrotalcite sample, used as filler.

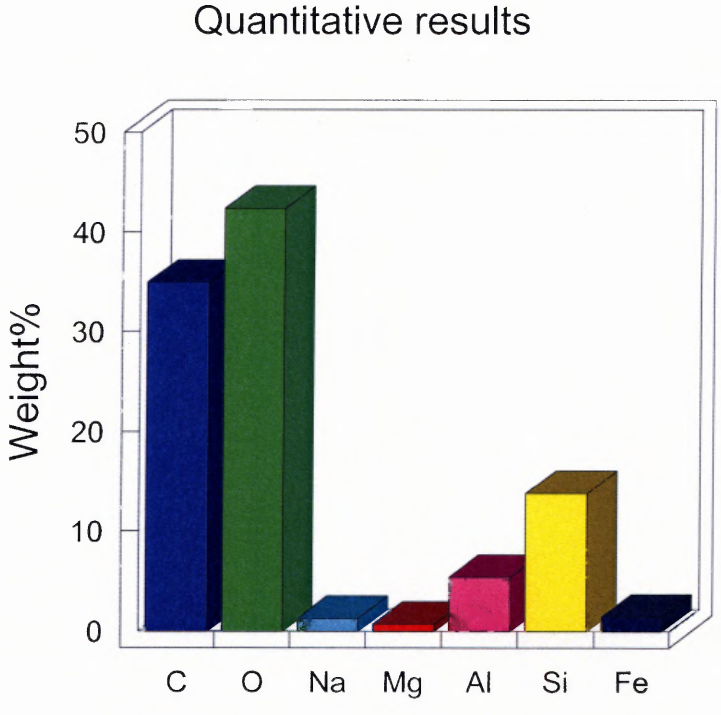

Figure A.2 EDX result of sodium montmorillonite sample, used as filler.

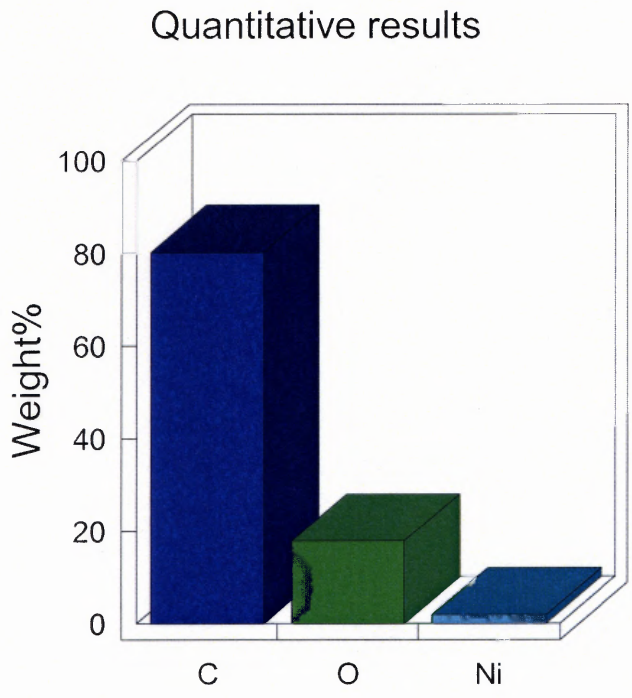

Figure A.3 EDX result of carbon nanotube sample, used as filler.

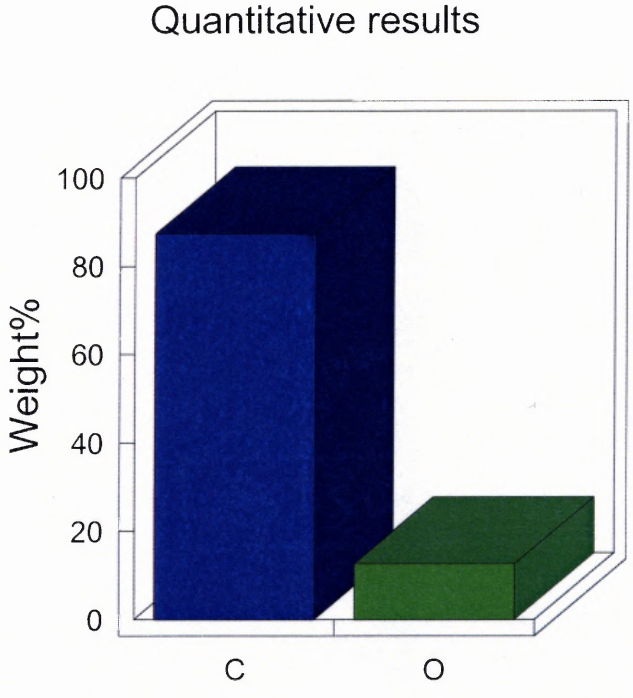

Figure A.4 EDX result of Fullerene sample, used as filler.

APPENDIX B

DIFFERENTIAL SCANNING CALORIMETRY THERMOGRAMS

In this Appendix, DSC thermograms of all the composites with and without fillers are presented.

Figures B.1 to B.5 present the DSC thermograms of PACR, PHT – 5, PMMT – 5, PSWNT – 5 and PFUL – 5, respectively. DSC was carried out using the Heat/Cool/Heat scan cycle. Results of only the first heat scan are in the Appendix since no additional information was obtained from any of the other cycles.

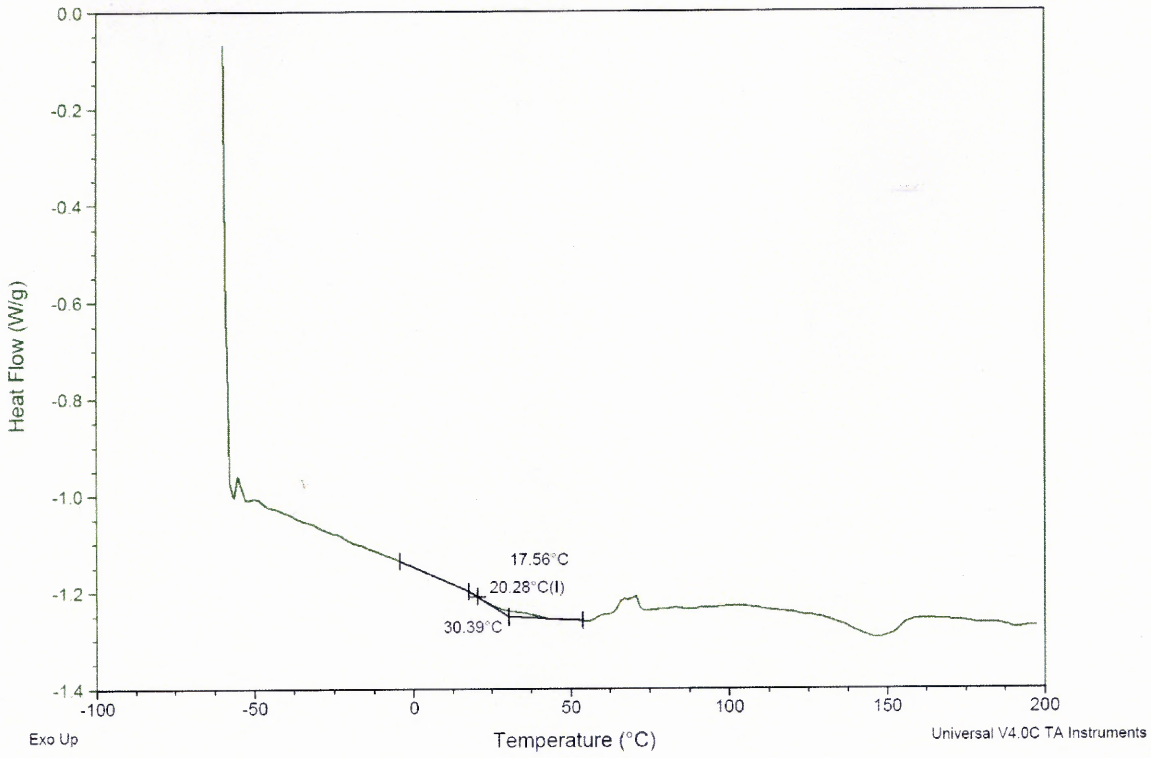

Figure B.1 DSC thermogram of PACR.

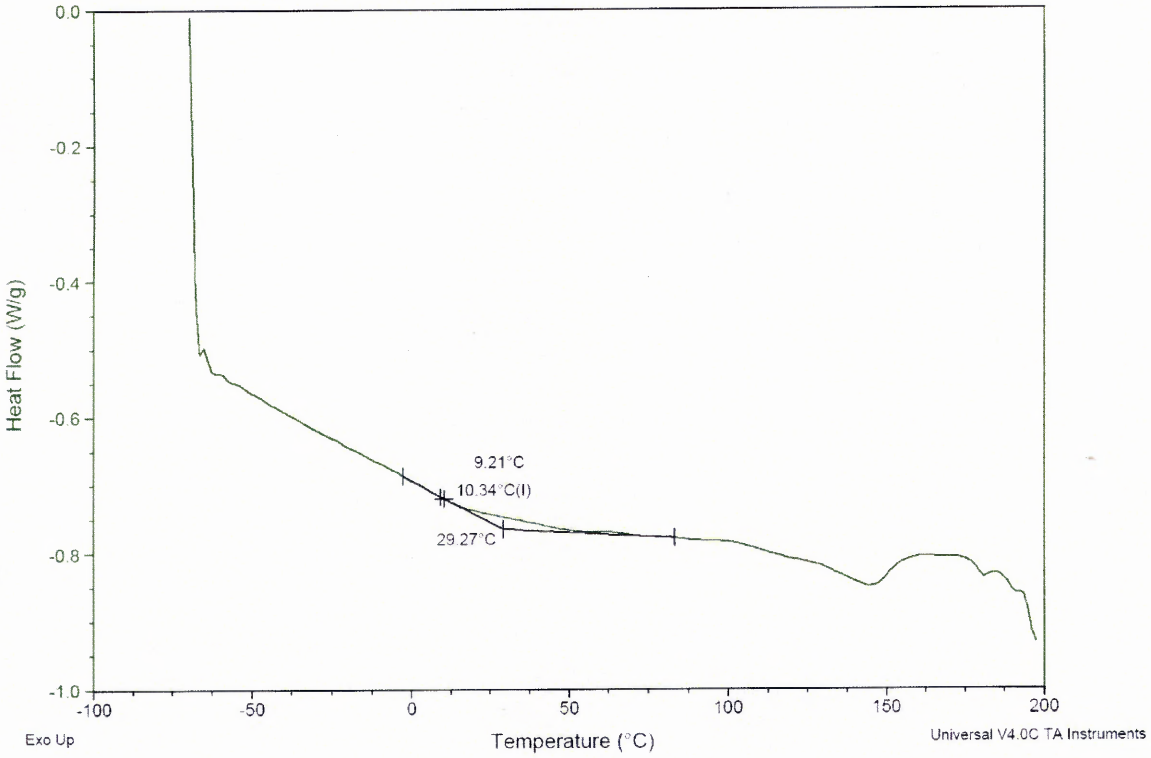

Figure B.2 DSC thermogram of PHT – 5.

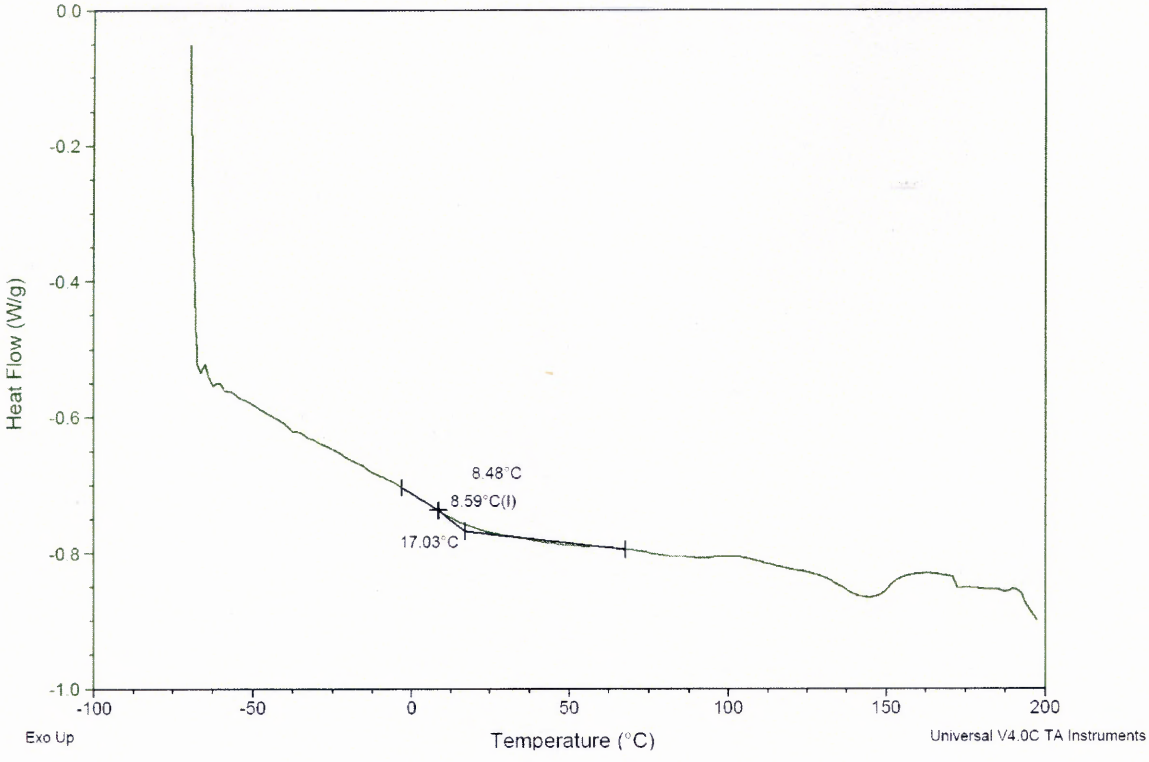

Figure B.3 DSC thermogram of PMMT – 5.

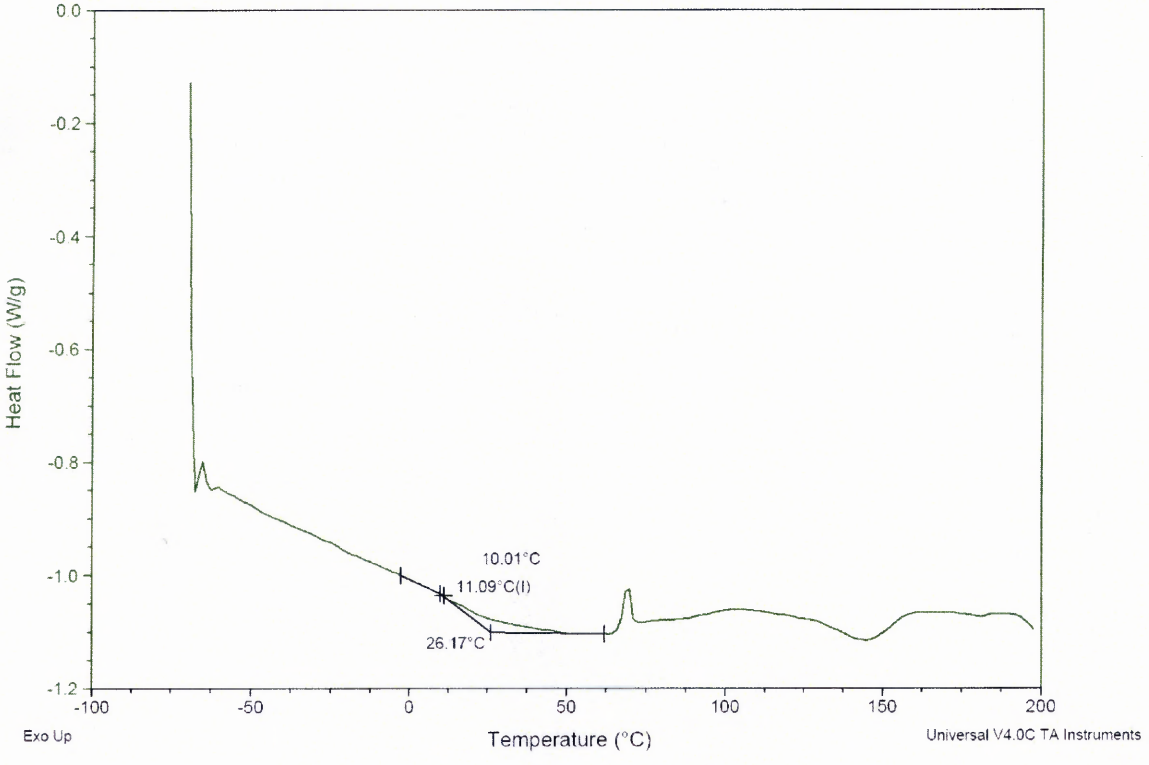

Figure B.4 DSC thermogram of PSWNT – 5.

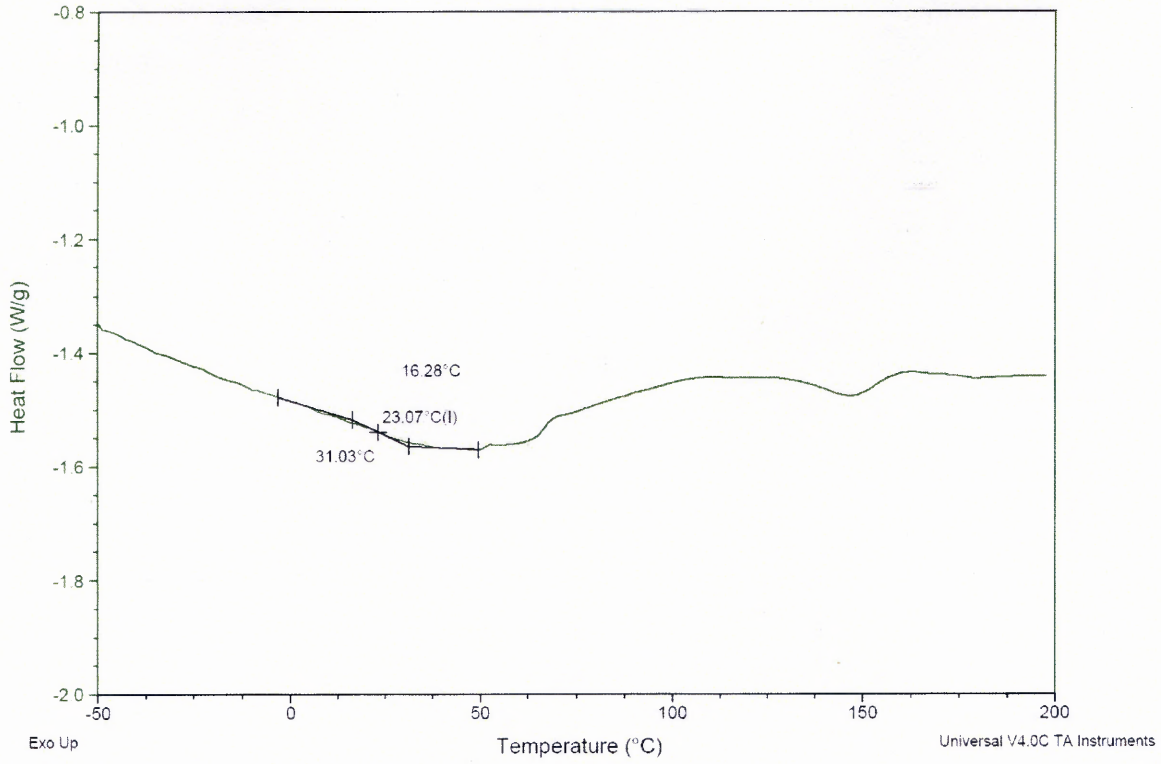

Figure B.5 DSC thermogram of PFUL – 5.

APPENDIX C

WATER VAPOR TRANSMISSION PLOTS

In this Appendix, the plots resulting from the water vapor transmission data for unfilled acrylic polymer and its composites with 5 wt% loading of nanofillers are presented. The plots of weight change vs. time are plotted and the slopes of the plots are also calculated in order to determine the water vapor transmission rate using Equation 3.6.

While Figures C.1 and C.2 present the plots obtained for the acrylic polymer without the fillers, Figures C.3 and C.4 present the plots of the composite containing 5 wt% hydrotalcite. Figures C.5 and C.6 present the plots of 5wt% sodium montmorillonite composite. Figures C.7 and C.8 present the plots of the composite containing 5 wt% carbon nanotubes and Figure C.9 presents the plot of the composite containing 5 wt% fullerene as the nanofiller.

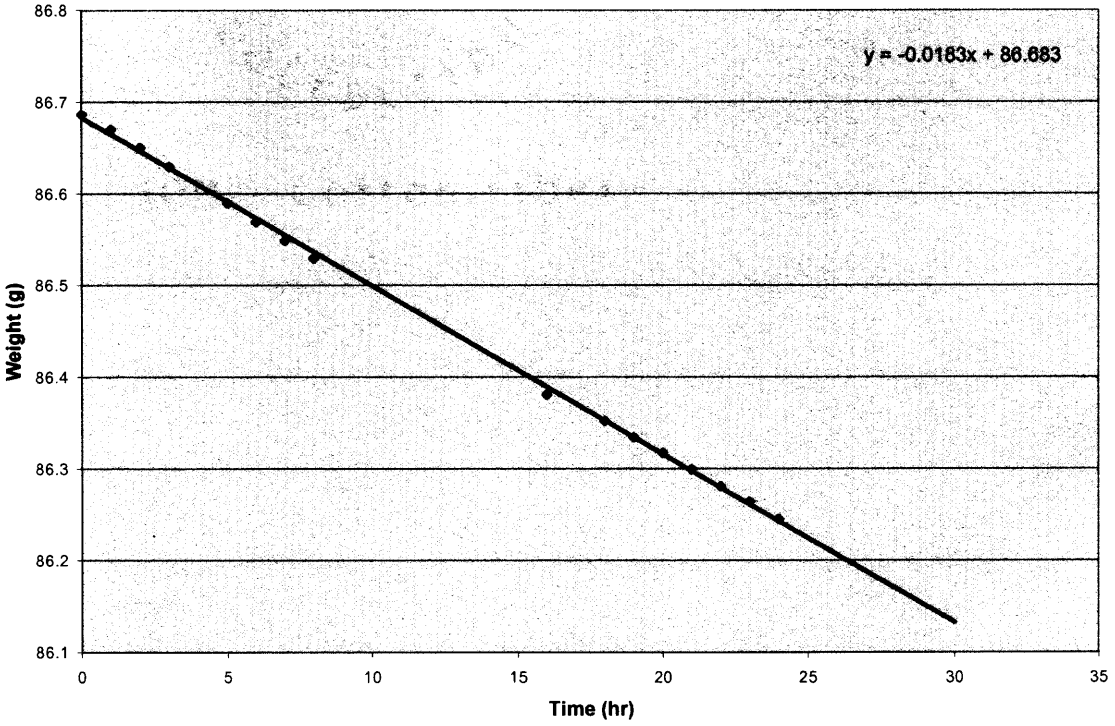

Figure C.1 WVT plot of PACR.

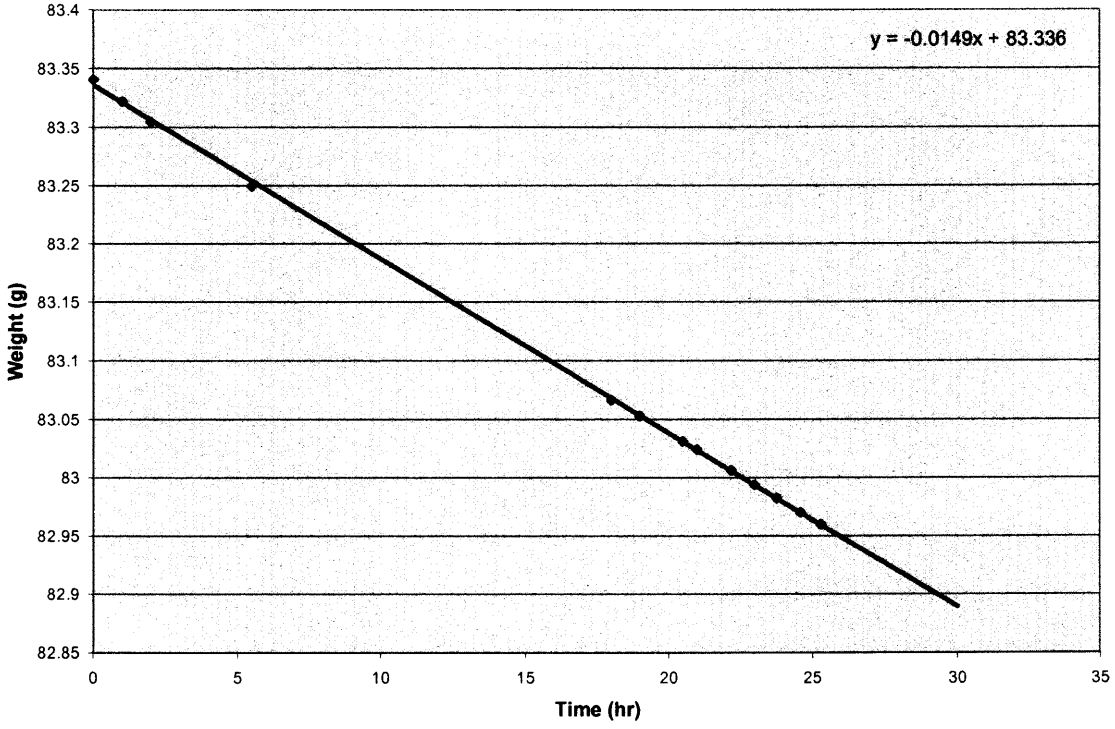

Figure C.2 WVT plot of PACR.

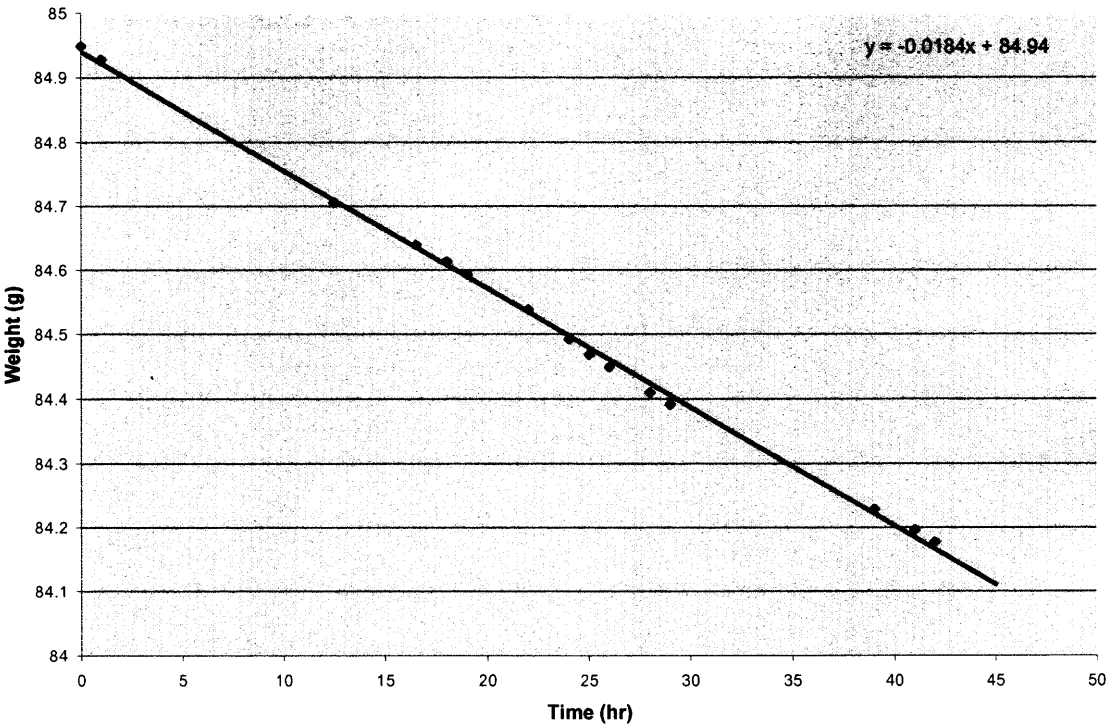

Figure C.3 WVT plot of PHT - 5.

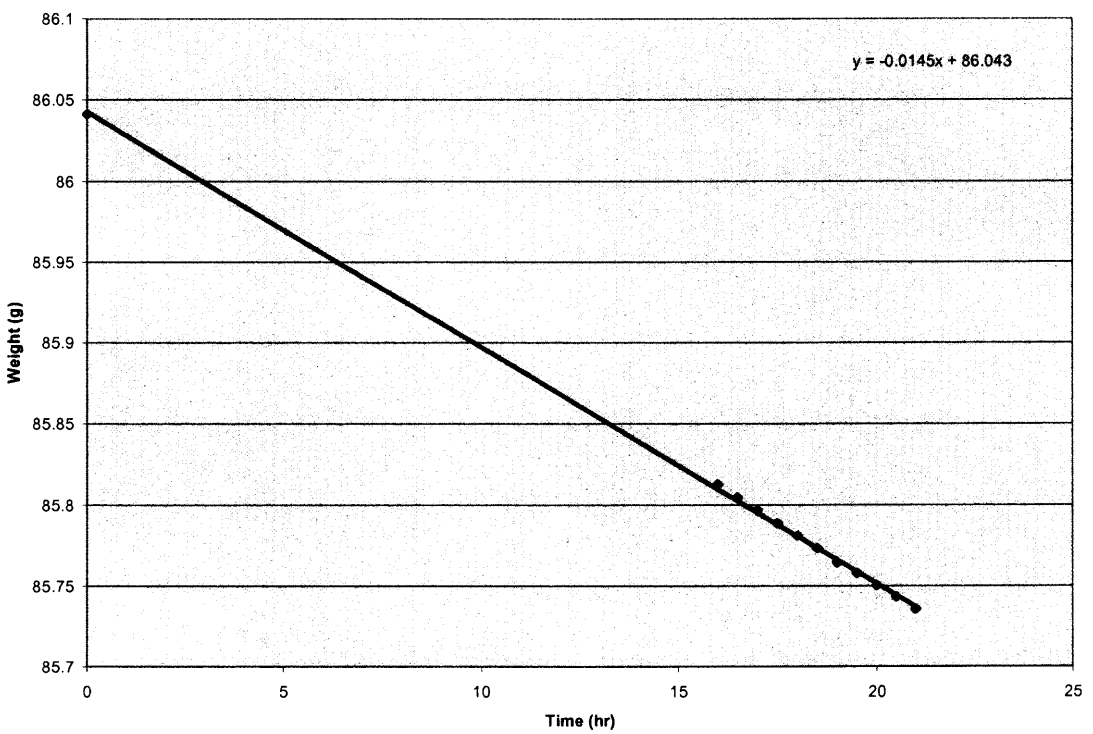

Figure C.4 WVT plot of PHT – 5.

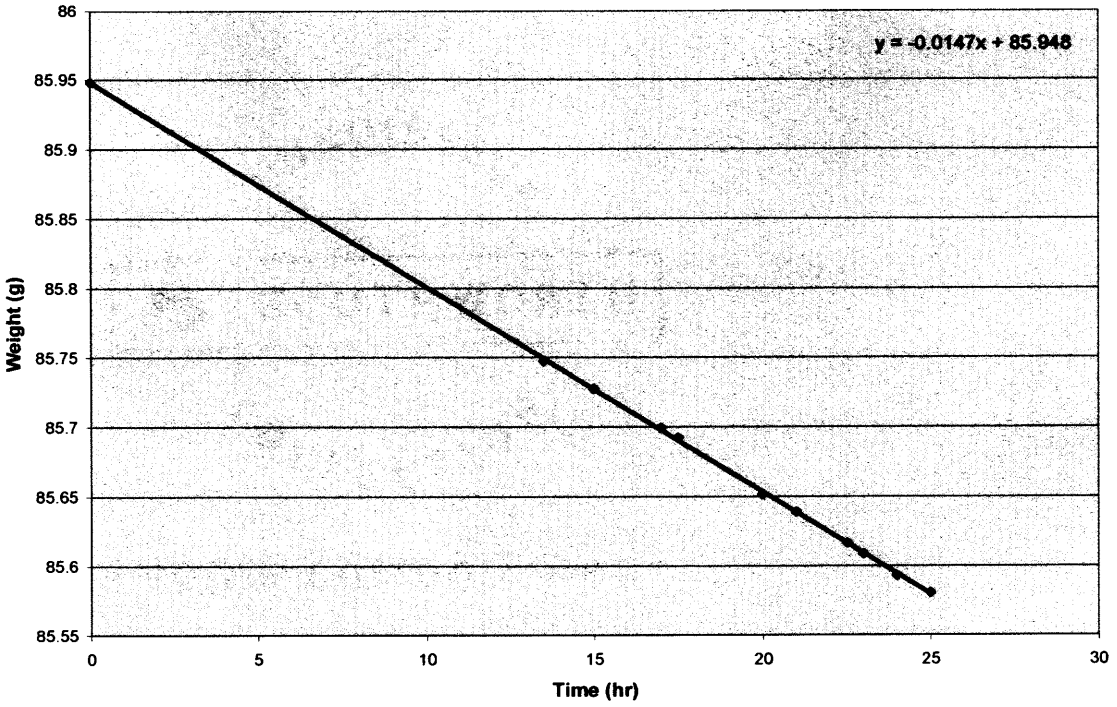

Figure C.5 WVT plot of PMMT - 5.

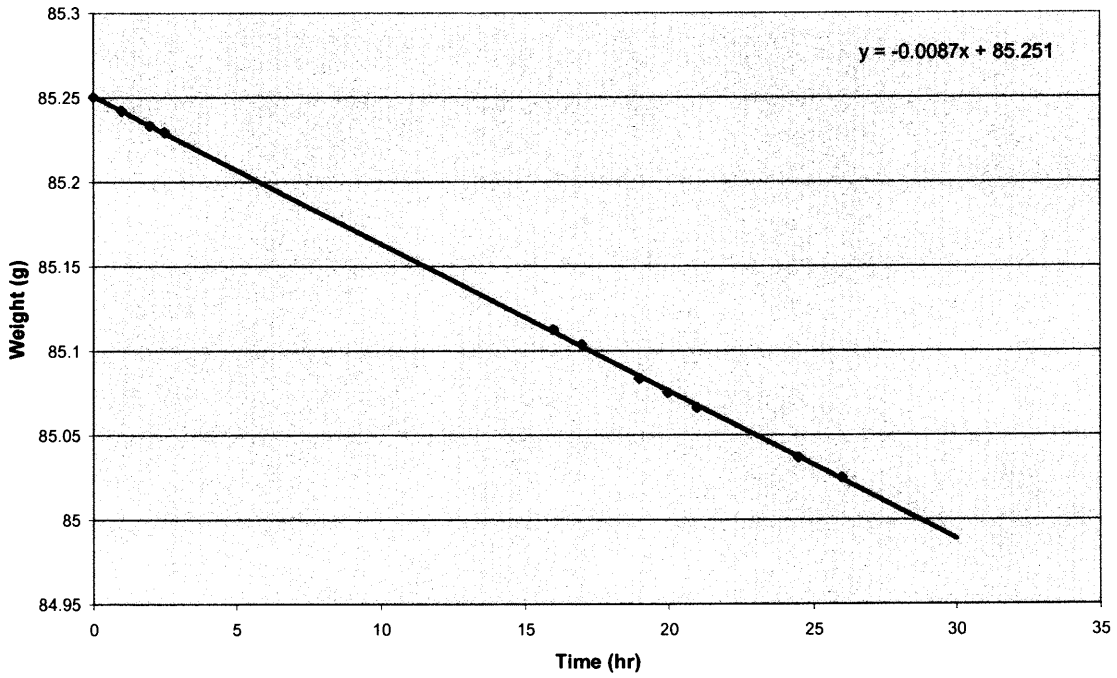

Figure C.6 WVT plot of PMMT - 5.

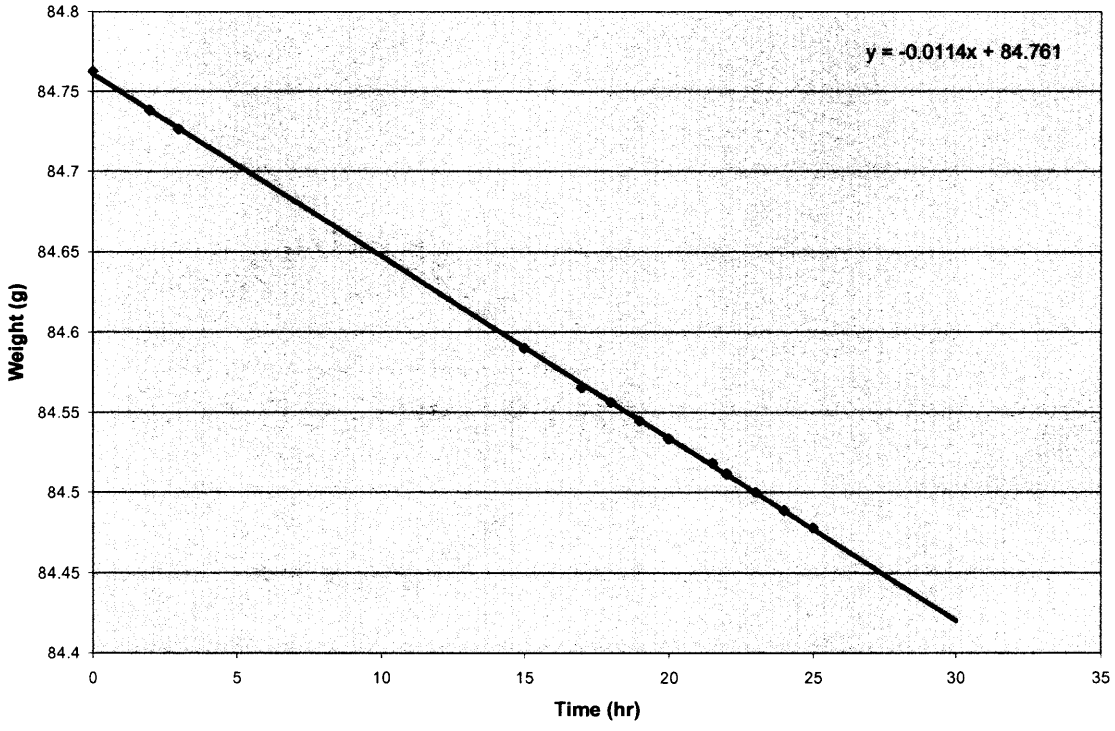

Figure C.7 WVT plot of PSWNT - 5.

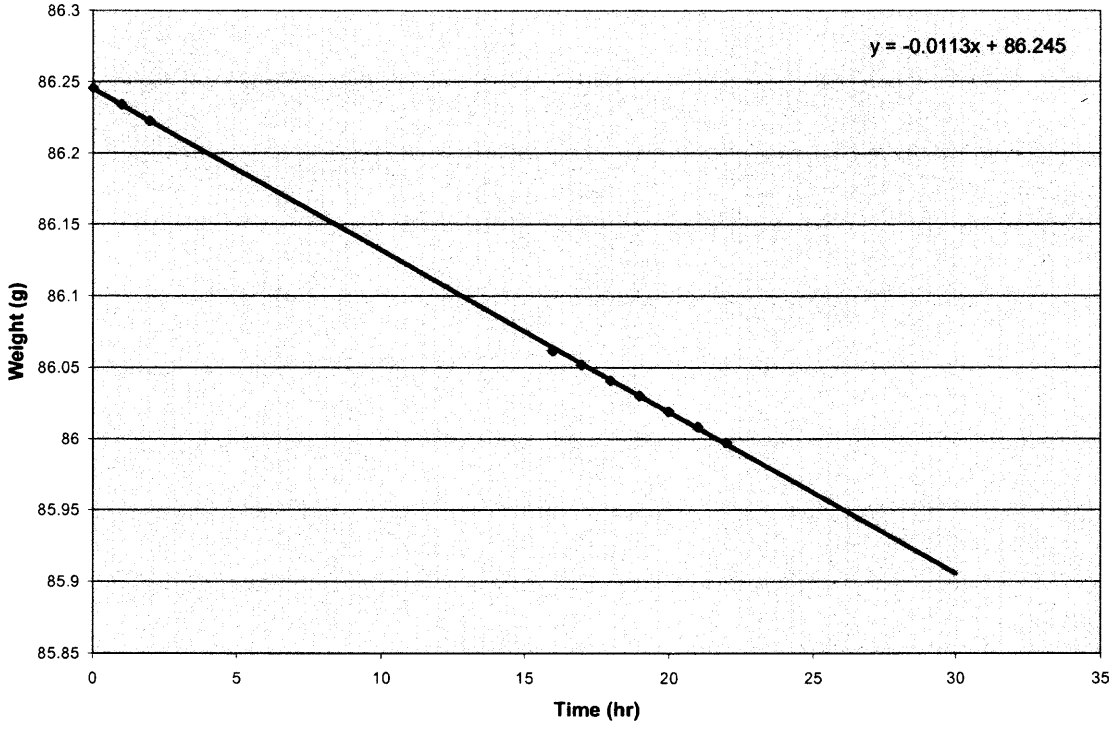

Figure C.8 WVT plot of PSWNT - 5.

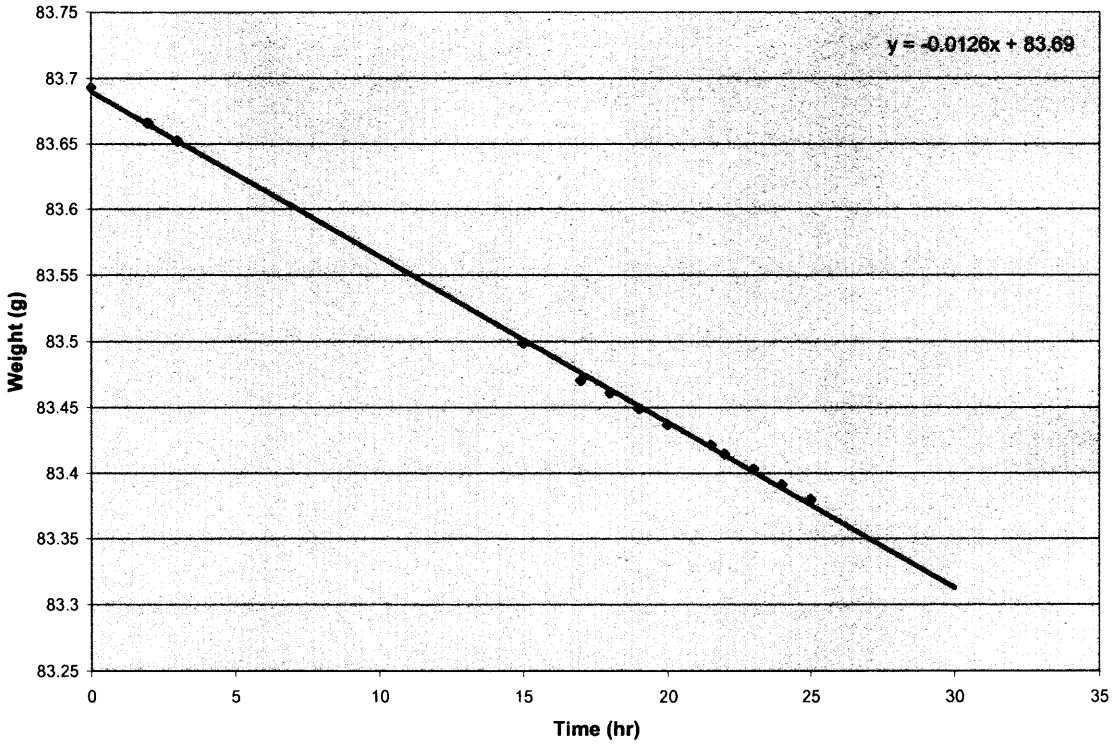

Figure C.9 WVT plot of PFUL - 5.

REFERENCES

Bratcher M., Gersten B., Ji H. and Mays J., "Study in the dispersion of carbon nanotubes", Materials Research Society Proceedings, 706, (2001).

Callister W. D., Fundamentals of Materials Science and Engineering, 2nd edition, John Wiley & Sons, Inc. (2005).

Carrado K. A., Xu L., Seifert S., Csencsits R. and Bloomquist C. A. A., "Polymer – clay Nanocomposites Derived from Polymer – Silicate Gels", Polymer – clay nanocomposites, Edited by Pinnavaia T. J. and Beall G. W., John Wiley & Sons Ltd. (2000).

Chang J. H., An Y. U., Cho D. and Giannelis E. P., "Poly(lactic acid) nanocomposites: comparison of their properties with montmorillonite and synthetic mica (2)", Polymer, 44, 3715 (2003).

DeGaspari J., "Eye on the future: Nanotechnology", Mechanical Engineering (2001), Retrieved July 2005 from the World Wide Web: http://www.memagazine.org/backissues/april01/features/prospect/prospect.html.

Delozier D. M., Watson K. A., Smith J. G. and Connell J. W., "Preparation and characterization of space durable polymer nanocomposite films", Composites Science and Technology, 65, 749 (2005).

Dubrovsky R. and Bezmelnitsyn V., "Bulk production of nanocarbon allotropes by a gas outflow discharge approach", Carbon, 42, 1861 (2004).

Edelstein A. S. and Cammarata R. C., Nanomaterials: Synthesis, Properties and Applications, Bristol; Philadelphia: Institute of Physics Pub. (1998).

Goyal A., "Role of Catalyst and substrate on synthesis of single wall carbon nanotubes", Thesis, New Jersey Institute of Technology, 2003.

Haggenmueller R., Gommans H. H., Rinzler A. G., Fischer J. E. and Winey K. I., "Aligned single – wall carbon nanotubes in composites by melt processing methods", Chemical Physics Letters, 330, 219 (2000).

Iijima S., "Helical microtubules of graphitic carbon", Nature, 354, 56 (1991).

Iqbal Z. and Goyal A., "Carbon Nanotubes/Nanofibers and Carbon Fibers", Functional Fillers for Plastics, Edited by Xanthos M., Wiley – VCH Verlag GmbH & Co. KGaA (2005).

Jiang L., Gao L. and Sun J., "Production of acqueous colloidal dispersions of carbon nanotubes", Journal of Colloid and Interface science, 260, 89 (2003).

Jiang T., Wang Y., Yeh J. and Fan Z., "Study on solvent permeation resistance properties of nylon6 / clay nanocomposite", European Polymer Journal, 41, 459 (2005).

Jin Z., Pramoda K. P., Xu G. and Goh S. H., "Dynamic mechanical behavior of melt – processed multi – walled carbon nanotube / poly(methyl methacrylate) composites", Chemical Physics Letters, 337, 43 (2001).

Jordan J., Jacob K. I., Tannenbaum R., Sharaf M. A. and Jasiuk I., "Experimental trends in polymer nanocomposites – a review", Materials Science and Engineering A, 393, 1 (2005).

Kiersnowski A., Dabrowski P., Budde H., Kressler J. and Piglowski J., "Synthesis and structure of poly(ε–caprolactone) / synthetic montmorillonite nano – intercalates", European Polymer Journal, 40, 2591 (2004).

Kymakis E., Alexandou I. and Amaratunga G. A. J., "Single – walled carbon nanotube – polymer composites: electrical, optical and structural investigation", Synthetic Metals, 127, 59 (2002).

Ma H., Zeng J., Realff M. L., Kumar S. and Schiraldi D. A., "Processing, structure, and properties of fibers from polyester / carbon nanofiber composites", Composites Science and Technology, 63, 1617 (2003).

Matayabas J. C. Jr. and Turner S. R., "Nanocomposite Technology for Enhancing the Gas Barrier of Polyethylene Terephthalate", Polymer – clay nanocomposites, Edited by Pinnavaia T. J. and Beall G. W., John Wiley & Sons Ltd. (2000).

Minami N., "Thin films of highly oriented single – wall carbon nanotubes", AIST Today, 2 (2002), Retrieved August 2005 from the World Wide Web: http://www.aist.go.jp/aist_e/aist_today/2003_07/2003_07_p25.pdf.

Osman M. A., Rupp J. E. P. and Suter U. W., "Tensile properties of polyethylene – layered silicate nanocomposites", Polymer, 46, 1653 (2005).

Park C., Ounaies Z., Watson K. A., Crooks R. E., Smith J. Jr., Lowther S. E., Connell J. W., Siochi E. J., Harrison J. S. and Clair T. L. St., "Dispersion of single wall carbon nanotubes by in situ polymerization under sonication", Chemical Physics Letters, 364, 303 (2002).

Patel S. H., "Processing Aids", Functional Fillers for Plastics, Edited by Xanthos M., Wiley – VCH Verlag GmbH & Co KGaA (2005).

Pinnavaia T. J. and Beall G. W., Editors: Polymer – clay nanocomposites, John Wiley & Sons Ltd. (2000).

Qian D., Dickey E. C., Andrew R. and Rantell T., "Load transfer and deformation mechanisms in carbon nanotube – polystyrene composites", Applied Physics Letters, 76, 2868 (2000).

Ray S. S., Okamoto M., "Polymer/layered silicate nanocomposites: a review from preparation to processing", Progress in Polymer Science, 28, 1539 (2003).

Schadler L.S., "Polymer-based and polymer-filled nanocomposites", Nanocomposite Science and Technology, Ajayan P.M., Schadler L.S. and Braun P.V., Wiley – VCH Verlag GmbH & Co. KGaA (2003).

Shaffer M. S. P. and Windle A. H., "Fabrication and characterization of carbon nanotube / poly(vinyl alcohol) composites", Advanced Materials, 11, 937 (1999).

Sorrentino A., Gorrasi G., Tortora M., Vittoria V., Costantino U., Mormottini F., "Incorporation of Mg – Al hydrotalcite into a biodegradable Poly(ε-caprolactone) by high energy ball milling", Polymer, 46, 1601 (2005).

Thostenson E. T. and Chou T. W., "Aligned multi – walled carbon nanotube – reinforced composites: processing and mechanical characterization", Journal of Physics D: Applied Physics, 35, L77 (2002).

Vaia R. A. and Wagner H. D., "Framework for nanocomposites", Materialstoday, 32 (November 2004).

Velasco J. I, Ardanuy M., Realinho V. and Gordillo A., "Preperation and characterization of polyolefine/hydrotalcite nanocomposites", Proc. of the Eurofillers Conf. (2005).

Wagenknecht U. and Costa F. R., "Flame Retardancy with Reinforcing Fillers – a New way of Materials design", Proc. of PPS – 21 Conf. (2005).

Xanthos M., "Modification of polymer Mechanical and Rheological Properties with Functional Fillers", Functional Fillers for Plastics, Edited by Xanthos M., Wiley – VCH Verlag GmbH & Co KGaA (2005).

Xanthos M., "Polymers and Polymer Composites", Functional Fillers for Plastics, Edited by Xanthos M., Wiley – VCH Verlag GmbH & Co KGaA (2005).

Zhao C., Hu G., Justice R., Schaefer D. W., Zhang S., Yang M. and Han C. C., "Synthesis and characterization of multi – walled carbon nanotubes reinforced polyamide 6 via in situ polymerization", Polymer, 46, 5125 (2005).

Zuev V. V., Bertini F. and Audisio G., "Fullerene C_{60} as stabilizer for acrylic polymers", Polymer Degradation and Stability, 90, 28 (2005).